SEISMIC VULNERABILITY ASSESSMENT OF SCHOOLS DESIGNATED AS POST-DISASTER SHELTERS IN MONTRÉAL

by

Ghaleb DAMAJ

THESIS PRESENTED TO ÉCOLE DE TECHNOLOGIE SUPÉRIEURE
IN PARTIAL FULFILLMENT FOR A MASTER'S DEGREE
WITH THESIS IN CONSTRUCTION ENGINEERING
M.A.Sc

MONTRÉAL, JULY 15, 2020

ÉCOLE DE TECHNOLOGIE SUPÉRIEURE
UNIVERSITÉ DU QUÉBEC

BOARD OF EXAMINERS

THIS THESIS HAS BEEN EVALUATED

BY THE FOLLOWING BOARD OF EXAMINERS

Rola Assi, Thesis Supervisor
Department of Construction Engineering, École de technologie supérieure

Ghyslaine McClure, Thesis Co-supervisor
Department of Civil Engineering and Applied Mechanics, McGill University

Richard Arsenault, President of the Board of Examiners
Department of Construction Engineering, École de technologie supérieure

Ahmad Abo El Ezz, Member of the jury
Scientific researcher, Geological Survey of Canada, Natural Resources Canada

THIS THESIS WAS PRENSENTED AND DEFENDED

IN THE PRESENCE OF A BOARD OF EXAMINERS

JUNE 22, 2020

AT ÉCOLE DE TECHNOLOGIE SUPÉRIEURE

ACKNOWLEDGMENT

I would like to express the deepest appreciation to my supervisor, Professor Rola Assi (ÉTS) and my co-supervisor Professor Ghyslaine McClure (McGill University) for their guidance and encouragement. The completion of this work could not have been possible without their participation and assistance. I am extremely grateful to them for providing such a nice support which made me complete this project.

I would like to acknowledge the financial support of Professor Rola Assi and the Centre d'études interuniversitaire des structures sous charges extrêmes (CEISCE).

Finally, I would like to thank my family, for their enduring support and their help, either directly or indirectly with my graduate studies.

Évaluation de la vulnérabilité sismique des écoles désignées comme des abris d'urgence à Montréal

Ghaleb DAMAJ

RÉSUMÉ

Ce projet vise à évaluer le risque sismique associé aux composants non structuraux (CNS) – aussi connus au Canada sous le nom de composants fonctionnels et opérationnels (CFO), dans 16 écoles désignées comme des abris post-catastrophe à Montréal par le Centre de sécurité civile de Montréal. Un indice déterministe amélioré de vulnérabilité structurale (VI) est déterminé par le processus d'analyse hiérarchique (PAH) en tenant compte des principaux paramètres structuraux considérés lors d'une étude précédente réalisée à l'Université McGill. L'étude précédente était réalisée sur la base d'inspection visuelle des bâtiments adaptée de la méthode américaine FEMA 154 (Federal Emergency Management Agency) et de la norme de conception parasismique des bâtiments de Nouvelle-Zélande. Les principaux paramètres considérés sont le type de système de résistance aux charges latérales, la hauteur du bâtiment, son année de construction, la présence d'irrégularités structurales (verticales et horizontales), ainsi que la sismicité et la classe de sol du site local définies dans le code national du bâtiment du Canada (CNB). La méthode PAH est appliquée pour estimer un facteur de pondération pour chacun des paramètres affectant la vulnérabilité sismique du bâtiment via une comparaison par paire de leur contribution afin d'améliorer l'équation de la vulnérabilité structurale proposée dans la norme CSA S832- *Réduction du risque sismique associé à la défaillance des composants fonctionnels et opérationnels des bâtiments*. Les résultats du nouvel indice de vulnérabilité ont été calibrés avec les résultats d'une étude précédente entreprise à l'Université McGill. Cette étape est suivie par l'intégration de l'effet de la résonance sol-superstructure en tant que nouveau paramètre dans l'évaluation de la vulnérabilité structurale à l'aide de la méthode PAH. Le nouveau VI est également classifié selon une échelle révisée qui contient quatre niveaux d'intensité : faible, modéré, élevé et très élevé. L'ajout du paramètre de résonance a augmenté la classe de vulnérabilité sismique dans certains cas. Enfin, le risque sismique associé aux CFO est évalué selon la norme CSA S832 en utilisant le VI amélioré. Conformément à cette norme, le risque sismique est évalué par le calcul d'un indice de risque (R) tenant en compte la vulnérabilité du bâtiment, l'aléa sismique du site, la vulnérabilité du composant en fonction de son mode d'attache à la structure, la possibilité de choc, martelage et renversement du CFO, sa flexibilité et son emplacement dans le bâtiment, ainsi que les conséquences liées à la rupture ou la non-fonctionnalité du CFO. Les résultats de l'indice de risque sont classifiés selon la même échelle que celle du CSA S832.

Mots-clés: Risque sismique, PAH, résonance sol-structure, indice de vulnérabilité, CFO, composants non structuraux.

Seismic vulnerability assessment of schools designated as post-disaster shelters in Montréal

Ghaleb DAMAJ

ABSTRACT

This research aims to assess the seismic risk associated to the non-structural components (NSCs), also known in Canada as operational and functional components (OFCs), of 16 schools designated as post-disaster shelters in Montréal by the Civil Safety Department of the City of Montréal. An improved deterministic structural vulnerability index (VI) is calculated using the Analytical Hierarchy Process (AHP). The new VI considers the main structural parameters considered in a previous study conducted at McGill University using the seismic screening method adapted from the American FEMA 154 (*Federal Emergency Management Agency*) and New Zealand guidelines. The main parameters include the type of lateral load resisting system, the building height, the year of construction, the presence of structural irregularities (vertical and horizontal), as well as the seismicity and soil class at the site as prescribed by the seismic design provisions of the National Building Code of Canada (NBC). The AHP method is applied to estimate a weight factor for each parameter contributing in the structural vulnerability via a pairwise comparison, in order to develop an improved structural vulnerability equation. The new vulnerability index is calibrated with the results of the previous study at McGill University. This calibration is followed by the integration of the effect of soil-building resonance as a new parameter in the assessment of the structural vulnerability currently proposed in the CSA S832 standard (*Seismic risk reduction of operational and functional components*). The new VI is classified into four categories: low, moderate, high and very high. The addition of the soil-building resonance parameter has increased the building seismic structural vulnerability classes in some cases. Finally, the seismic risk associated to the OFCs is assessed based on the improved structural vulnerability index and the CSA S832 parametric method based on onsite inspection. Accordingly, the evaluation of the seismic risk is represented by calculating a risk index (R) that takes into consideration the vulnerability of the building, the seismic hazard at the building site and the vulnerability of the component based on the OFC restraint, impact and pounding, OFC overturning and OFC flexibility and location in building, in addition to the consequences of OFC failure or lack of functionality. The risk indices are classified according to the mitigation priority thresholds of CSA S832.

Keywords: Seismic risk, AHP, soil-building resonance, seismic screening method, OFC, non-structural components

TABLE OF CONTENTS

Page

INTRODUCTION 1

CHAPTER 1 LITERATURE REVIEW 5
1.1 Seismic performance of school buildings and their OFCs during past high magnitude earthquakes 5
1.2 Seismic vulnerability and assessment methods 6
1.2.1 Quantitative assessment methods 9
1.2.2 Qualitative assessment methods 21
1.3 Previous studies on post-earthquake functionality of buildings 36
1.4 Previous studies on the effects of soil-structure resonance 39
1.5 Analytical Hierarchy Process (AHP) 41

CHAPTER 2 SEISMIC STRUCTURAL VULNERABILITY OF SCHOOLS IN MONTRÉAL CONSIDERING THE EFFECT OF SOIL-BUILDING RESONANCE 46
2.1 School building databases 47
2.2 Reliability of the ambient vibration measurement test results 48
2.3 Coefficient of soil-building resonance 49
2.4 Vulnerability index from AHP 51
2.5 Validation of vulnerability index using AHP 53
2.6 Limitations 57

CHAPTER 3 NEW OFC SEISMIC RISK INDEX ACCORDING TO THE CSA S832 METHOD 58
3.1 Setting building vulnerability index limits 58
3.2 Improvement of the OFC seismic risk index with effect of the variation of the local seismicity 59
3.3 New OFC seismic risk index for a case study building in Montréal 60
3.3.1 Drift-sensitive components 61
3.3.2 Acceleration-sensitive components 64
3.4 Effect of the seismicity on the OFC seismic risk 66
3.5 Observations 70

CHAPTER 4 SUMMARY AND CONCLUSIONS 71
4.1 New seismic structural vulnerability index 71
4.2 New OFC seismic risk index 72
4.3 Conclusions 72
4.4 Suggestions for future work 74

APPENDIX I CHARACTERISTICS OF SCHOOL BUILDINGS IN MONTRÉAL 75

APPENDIX II DYNAMIC PROPERTIES OF THE STUDIED BUILDINGS AND THE ADJACENT SOIL 86

APPENDIX III VALIDATION OF THE AHP RESULTS WITH THE ADAPTED SEISMIC SCREENING METHOD 91

APPENDIX IV DETAILED APPLICATION OF THE AHP-BASED METHOD AND THE ADAPTED SCREENING METHOD 99

LIST OF BIBLIOGRAPHICAL REFERENCES 101

LIST OF TABLES

Page

Table 1.1 Types of Lateral Load Resisting Systems according to FEMA 154.....24

Table 1.2 Collapse rates by model building type for complete structural damage...25

Table 1.3 Basic score and score modifiers according to Tischer's adapted screening method.....26

Table 1.4 Basic score and score modifiers according to Tischer's adapted screening method.....27

Table 1.5 Seismic vulnerability ranking system used in Oregon with FEMA 154 ...28

Table 1.6 Damage functions for seismic screening in Eastern Canada 28

Table 1.7 Ground motion amplification factors for Montréal, according to NBC 2015.....29

Table 1.8 Building characteristics index according to CSA S832-14.....32

Table 1.9 Individual OFC parameters and weight factors according to CSA S832-14 33

Table 1.10 Rating scores for OFC characteristic index according to CSA S832-14 ..34

Table 1.11 Rating scores used for the determination of the consequence index of OFCs according to CSA S832-14 35

Table 1.12 Suggested mitigation priority thresholds according to CSA S832-14 36

Table 1.13 AHP scale of preference between two parameters 42

Table 1.14 AHP random consistency indices (RI).....43

Table 2.1 Priority and normalized weights of five parameters from the adapted screening method according to AHP 52

Table 2.2 Priority and normalized weights of five parameters including the coefficient of resonance according to AHP 52

Table 2.3 Structural vulnerability classes according to the proposed method.....53

Table 2.4 Characteristics of eight concrete buildings (School 16 in Appendix I).....54

Table 2.5 Comparison of structural vulnerability indices and classes according to the AHP-based method and Tischer's adapted screening method without the coefficient of resonance 54

Table 2.6 Comparison of structural vulnerability index and class according to the AHP-based method with consideration of the coefficient of soil-building resonance for a school campus with 8 buildings 55

Table 2.7 Comparison of Structural vulnerability index and class according to the AHP-based method considering soil-building resonance and Tischer's adapted screening method for two buildings (School 1 in Appendix I) 56

Table 2.8 Comparison of the vulnerability class according to the AHP-based method considering soil-building resonance and Tischer's adapted screening for a school campus of 6 buildings (School 6 in Appendix I)...56

Table 3.1 Characteristics of the case study school building (School 16 in Appendix I). 60

Table 3.2 Drift-sensitive components located in Building T 62

Table 3.3 Comparison of the improved seismic risk index of the critical drift-sensitive components with the existing risk according to CSA S832.....63

Table 3.4 Suggested mitigation priority thresholds according to CSA S832 64

Table 3.5 Critical acceleration-sensitive components located in Building T 65

Table 3.6 Comparison of the improved seismic risk index of the critical acceleration-sensitive components.....65

Table 3.7 Improved seismic risk index, R, for drift-sensitive components with different seismicity.....67

Table 3.8 Seismic risk index, R, according to CSA S832 for drift-sensitive components with different seismicity 68

Table 3.9 Improved seismic risk index, R, for acceleration-sensitive components with different seismicity 69

Table 3.10 Seismic risk index, R, according to CSA S832 for acceleration-sensitive components with different seismicity 70

LIST OF FIGURES

Page

Figure 1.1 Operational and Functional Components (OFCs) in buildings.....7

Figure 1.2 Relative direct costs of building components according to use and occupancy 8

Figure 1.3 Nonlinear static analysis procedure 10

Figure 1.4 Schematic of Static Pushover Analysis used in the Capacity Spectrum Method 11

Figure 1.5 Graphical representation of the capacity spectrum method.....11

Figure 1.6 Flow Chart of NDA to Determine Seismic Building Response 13

Figure 1.7 Main steps of FRACAS for the derivation of the performance point (PP) using the trilinear idealization model.....15

Figure 1.8 Flowchart of the FaMIVE procedure.....17

Figure 1.9 Modules of HAZUS.....19

Figure 1.10 Fragility curves for slight, moderate, extensive and complete damage.....20

Figure 1.11 Example of a building capacity curve.....21

Figure 1.12 Analysis procedure in the building portfolio recovery model (BPRM) 37

Figure 1.13 Flowchart of the probabilistic approach of pre-recovery damage and functionality loss assessment 37

Figure 1.14 Building damage and utility availability to building functionality states..38

Figure 1.15 Effect of resonance on the seismic response of buildings 39

Figure 2.1 Distribution of LLRS for the evaluated schools using the adapted seismic screening method 47

Figure 2.2 Tromino sensor 48

Figure 2.3 Average fundamental frequency of the tested soil site 49

Figure 2.4 Distribution of coefficients of soil-building resonance for 69 buildings located in Montréal 50

LIST OF ABBREVIATIONS

ADRS	Acceleration-displacement response spectrum
AHP	Analytical hierarchy process
ATC	Applied Technology Council (United States)
AVM	Ambient vibration measurement
BHRC	Building housing research center (United States)
BPRM	Building portfolio recovery model
BSH	Basic structural hazard
CMF	Concrete moment frame
CIW	Concrete frame with infill masonry shear walls
CR	Consistency ratio
CoR	Coefficient of resonance
CSM	Capacity spectrum method
CSW	Concrete shear walls
DOF	Degree of freedom
FaMIVE	Failure mechanism identification and vulnerability evaluation
FEMA	Federal Emergency Management Agency (United States)
FRACAS	Fragility through capacity spectrum method
GIS	Geographic information system
HAZUS	Hazard United States Software
HVMWR	Horizontal-to-vertical moving window ratio
HVSR	Horizontal-to-vertical spectral ratio
LLRS	Lateral load resisting system
MCE	Maximum considered earthquake
NASW	Noise analysis of surface waves
NBC	National Building Code of Canada
NDA	Nonlinear dynamic analysis
NIBS	National Institute of Building Sciences

NRC	National Research Council of Canada
NSC	Nonstructural component
OFC	Operational and functional component
PCF	Precast concrete frame
PCW	Precast concrete walls
PESH	Potential earth science hazards
PGA	Peak ground acceleration
RI	Random consistency index
RMC	Reinforced masonry bearing walls with concrete diaphragm
RML	Reinforced masonry bearing walls with wood and metal deck floors
SBF	Steel braced frame
SCW	Steel frame with concrete shear walls
SDOF	Single degree of freedom
SIW	Steel frame with infill masonry shear walls
SLF	Steel light frame
SM	Score modifiers
SMF	Steel moment frame
SPI	Seismic priority index
STD	Standard deviation
STFT	Short time Fourier transform
URM	Unreinforced masonry bearing walls
VI	Vulnerability index
WLF	Wood light frame
WPB	Wood post-and-beam construction
WT	Wavelets transform

LIST OF SYMBOLS

A	Standard pseudo acceleration
C	Consequence score
D	Deformation spectrum ordinate
V	Vulnerability
R	Risk index
β_{eq}	Equivalent viscous damping ratio
Γ	Modal participation factor
F_a	Soil modification factor in NBC
F_0	Seismic force at OFC
M_1	Effective modal mass
S_a	Spectral acceleration
S_a (0.2)	Spectral acceleration at 0.2s
S_D	Spectral displacement
T_{eq}	Equivalent fundamental period
T_n	Natural period
V_b	Base shear
V_{s30}	Site shear wave velocity averaged over 30-m depth
t_0	Time of occurrence of scenario
V_B	Building characteristics index
V_E	OFC characteristics index
V_G	Ground motion characteristics vulnerability index
V_{total}	Total lateral load
μ_N	Top floor displacement
ϕ	Mode shape vector
M_{eff}	Tributary mass
K_{eff}	Lateral effective stiffness
λ	Load factor

INTRODUCTION

Previous studies and experience from past earthquakes have demonstrated that there is a need to assess the seismic vulnerability of school buildings even in zones of moderate seismicity (Dolce, 2004). One may recall the adverse performance of schools during the M_w 8.0 Sichuan (China) earthquake in 2008 that resulted in the deaths of hundreds of children while at school (Revkin, 2008). Although such severe earthquakes are not likely in Québec, school buildings remain potentially vulnerable to moderate shaking as many may have inadequate exit pathways, and students/pupils may not be able to exit safely and quickly enough when an emergency occurs (Rodgers, 2012). In Québec, most school buildings have structural irregularities, and many would likely have poor seismic performance if subjected to moderate to strong earthquakes because they were designed and built in the 1960s and 1970s, before the introduction of modern earthquake-resistant design procedures in the National Building Code of Canada (NBC). Another compelling reason to assess their seismic vulnerability is that school buildings (secondary school buildings in particular) are possible candidates to serve as post-critical shelters in case of disasters. Therefore, school buildings must remain structurally safe at all times (Chakos, 2004), hence the importance of adequately assessing their seismic vulnerability and post-earthquake functionality.

The present research contributes to a better assessment of seismic structural vulnerability and post-earthquake functionality of 16 schools designated as post-disaster shelters in Montréal by introducing the soil-building resonance as a parameter deemed to affect their vulnerability. The Analytical Hierarchy Process (AHP) is used to integrate this resonance parameter in the seismic structural vulnerability assessment of buildings, and to calibrate it with the adapted seismic screening method developed by Tischer (Tischer, 2012). Furthermore, the assessment of the seismic risk associated to the operational and functional components (OFCs) located in the schools is conducted by applying the method proposed in the CSA S832 standard (CSA, 2014) with an improved building structural vulnerability index, V_B, that considers soil-building resonance effects and structural irregularities.

Objective

The main objective of this study is to propose an improved method for assessing the post-earthquake functionality of school buildings designated as post-disaster shelters in Montréal. The post-earthquake functionality of a building depends both on its structural integrity and safety and on the integrity of its OFCs. The study recommends improving the parametric method proposed in CSA S832 for seismic risk assessment of OFCs by considering new parameters associated with structural irregularities of the lateral-load resisting system of the building, the year of construction, and the possible soil-building resonance effect. To account for the latter, a coefficient of resonance (CoR) is calculated and added to the evaluation of the building vulnerability index (V_B) using the AHP method.

Methodology

To achieve the main research objective, the applied methodology comprises the following steps:

1) Study of the existing information on school buildings designated as post-disaster shelters in Montréal, which forms the database of the current study.
2) Evaluation of the adapted seismic screening method proposed by Tischer (2012) and inspired by the rapid visual screening of buildings for potential seismic hazard (FEMA 154).
3) Extraction of the dynamic properties of 69 school buildings and local soil, such as the fundamental frequency and damping ratio of the structures.
4) Estimation of the coefficient of soil-building resonance by dividing the fundamental frequency of the adjacent soil by the fundamental frequency of the school building. The school buildings having a coefficient of resonance between 0.9 and 1.1 are classified as vulnerable to resonance.
5) Development of new vulnerability index using AHP, in order to evaluate the seismic structural vulnerability of schools considering possible soil-building resonance.

6) Estimation of a new OFC seismic risk index based on the CSA S832 parametric method using the new proposed structural vulnerability index.

Organization of the report

This report consists of four chapters. Chapter 1 provides background and a brief literature review of the performance of school buildings during past earthquakes and the previous methods used to assess the seismic structural and non-structural vulnerabilities as well as the effect of soil-building resonance on the seismic vulnerability. Chapter 2 presents the development of a new structural vulnerability index that considers the effect of soil-building resonance by applying the AHP method. Chapter 3 describes the estimation of the new seismic risk index based on the CSA S832 method and the application of the AHP method.

Finally, Chapter 4 states the original contributions of the current study as well as its impact and limitations and some recommendations for future work.

CHAPTER 1

LITERATURE REVIEW

The performance of school buildings during past earthquakes is reviewed next. In addition, this chapter presents the available rapid screening methods to assess seismic structural and non-structural vulnerabilities. The description of the adapted seismic screening method developed by Tischer (Tischer, 2012) and the CSA S832 (CSA, 2014) parametric method are reviewed in more detail as well as the theory of the Analytical Hierarchy Process (AHP).

1.1 Seismic performance of school buildings and their OFCs during past high magnitude earthquakes

The poor seismic performance of school buildings in many countries has made their vulnerability assessment and retrofit a priority in moderate and high seismic zones. According to the Building and Housing Research Center of the United States (BHRC, 2005), school buildings are considered as vital structures, so upgrading them to sustain the effects of strong earthquakes is highly important to reduce loss of life. The good seismic performance of OFCs is essential to ensure the building safety and functionality, especially in school buildings designated as post-disaster shelters.

The recent September 2017, M_w 7.1 earthquake in Mexico City has killed 22 people at a school that collapsed (Singh et al., 2018). In eastern Turkey, the city of Van has been hit by a M_w 7.1 earthquake on October 23, 2011, which caused the collapse of 58 buildings, including some schools, and 604 human deaths and more than 2000 injured (222 of them were rescued under the collapsed buildings) (Taskin et al., 2013) . Moreover, during the February 2010, M_w 8.8 earthquake in Chile, around 2000 schools were heavily damaged (Ghosh & Cleland, 2012). In Pakistan, the M_w 7.8 earthquake that hit Kashmir on October 8, 2005, has badly affected the three main districts facilities such as hospitals, schools and services including police and armed forces (Peiris et al., 2008). The earthquake occurred during day school time hours, with resulted in the tragic death of approximately 19000 pupils and students, most of them trapped

under the collapsed school buildings. Another example is the catastrophic M_w 9.3 earthquake and tsunami that struck Indonesia in 2004 and destroyed approximately 750 school buildings and damaged more than 2000 other, killing thousands of teachers and students (McAdoo et al., 2006). Built in 1960, the Iovene primary school in San Guiliano, Italy collapsed during the more moderate October 31, 2002 M_w 5.5 Molise earthquake, causing approximately 28 children deaths (Decanini et al., 2004). The amplification of the ground motion from the local soil conditions and poor unreinforced masonry construction have caused the collapse (Dolce, 2004). The 20 October 1999 M_w 7.6 earthquake that hit Chi-Chi in Taiwan caused the collapse of 51 schools while many other school buildings experienced considerable damage (Kelson et al., 2001). Moreover, the July 1997, M_w 6.8 earthquake in Caraico, Venezuela destroyed four school buildings; most of them were concrete frames with unreinforced infill masonry, and they collapsed due to their weak resistance and stiffness (López et al., 2007). To mention a few Canadian examples, the relatively moderate 1988 M_w 5.9 Saguenay earthquake caused architectural damage that cost several millions of Canadian dollars in repair and retrofit (Tinawi & Mitchell, 1990). A total of 16 of the 25 schools of the Chicoutimi public school board experienced severe architectural damage that cost around 3 million dollars to repair, and 17 schools of the Baie des Ha! Ha! School board also suffered severe architectural damage that cost 2.8 million dollars.

1.2 Seismic vulnerability and assessment methods

The seismic vulnerability of a building structure and its non-structural components is defined by their inability to resist the effects of earthquake-induced forces and displacements, thus jeopardizing life safety and building functionality. It is a global concept that can be sub-divided into seismic structural vulnerability (addressing life safety) and seismic vulnerability of its OFCs (addressing building functionality). The seismic vulnerability level can be evaluated and expressed by functions that can be derived either by statistical studies of damaged buildings in earthquakes or by simulations using analytical, probabilistic and numerical methods (Calvi et al., 2006).

Figure 1.1 shows typical building OFCs that are permanently or temporarily attached to the structure so that their seismic vulnerability is strongly affected by the quality and configuration of their anchoring to the supporting structure.

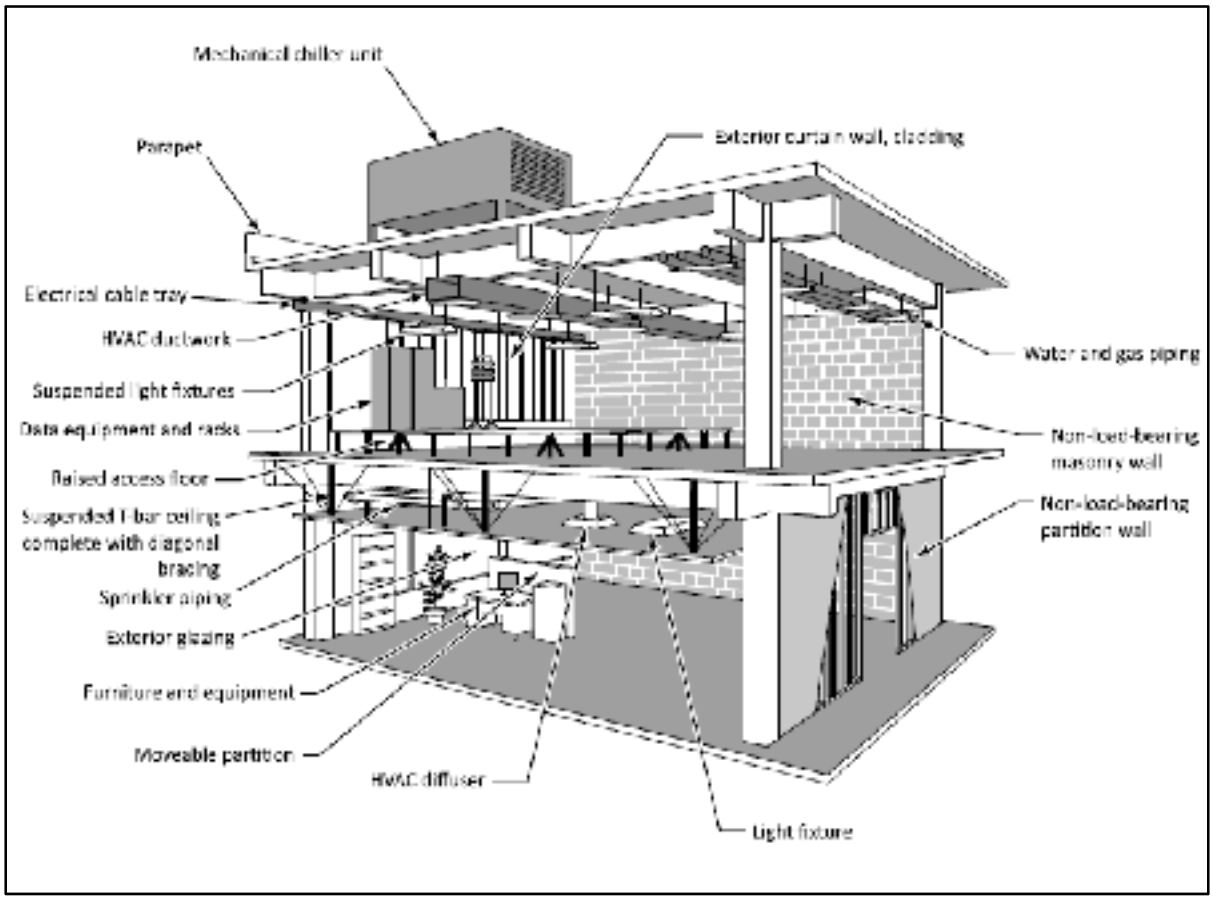

Figure 1.1 Operational and Functional Components (OFCs) in buildings
(Source: CSA S832-14 (2014))

Taghavi and Miranda (2003) noted that damage to OFCs yields the largest economic losses due to earthquakes; the cost of these components typically represents 60% to 90 % of the total construction cost for buildings with intended use and occupancy of office/schools, hotels and hospitals, as illustrated in Figure 1.2. In addition to the costs caused by direct damage to the components themselves, further losses are suffered as the building functionality is compromised, even if the structure is safe. The level of vulnerability of OFCs can be high if their restraints are inadequate and the OFCs are prone to instability that might cause

overturning and/or sliding. According to the parametric method of CSA S832 (CSA, 2014), the vulnerability index of OFCs depends on their location in the building and their connection with the structure, such as anchorage configuration and load path. The higher the vulnerability of these components, the higher the seismic risk, which is a function of the vulnerability and consequences. Overall, the risk is related to threats to life safety, loss of function and property loss. Moreover, the vulnerability of OFCs has direct consequences on the safe evacuation of buildings.

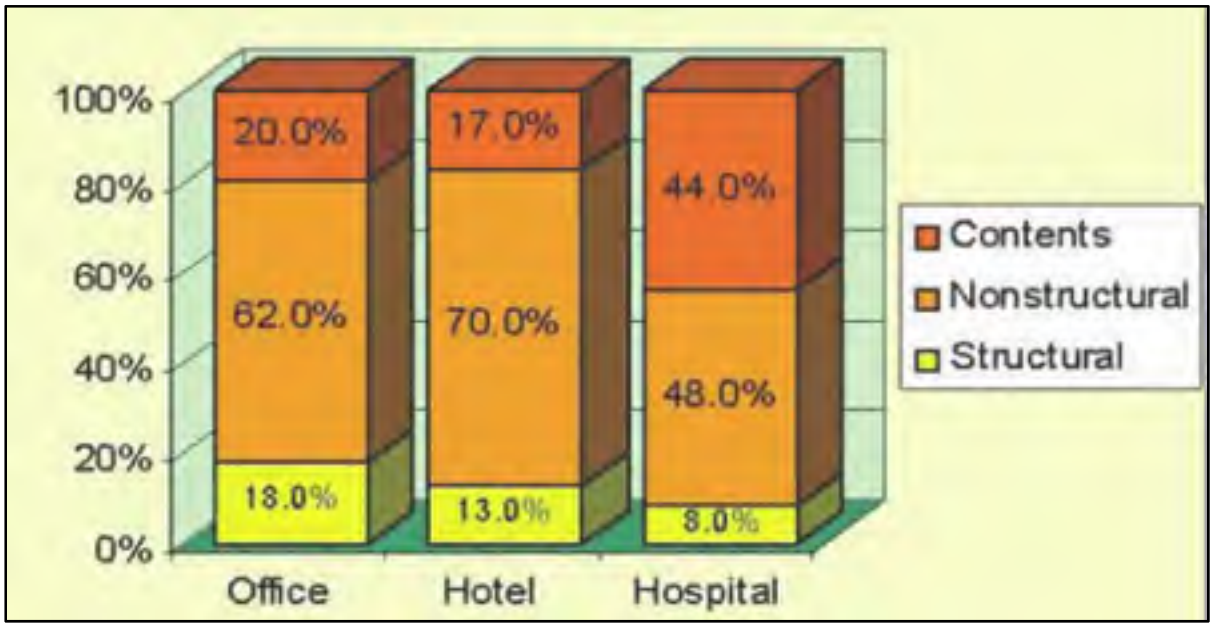

Figure 1.2 Relative direct costs of building components according to use and occupancy (Source: Taghabi & Miranda (2003))

Losses due to OFC damage can range from minor to severe depending on their use and replacement cost. For example, if the bookshelves in school libraries are not properly secured and restrained, they can topple without having a significant loss of function (or material losses), but they are a human life hazard if the premises are occupied during the earthquake.

Bertogg et al. (2002) noted that the loss analysis must focus at least on the basic vulnerability parameters that can be used in a typical risk model. It is extremely important to distinguish

between the more detailed assessment of individual buildings and the assessment of groups of buildings at the so-called urban scale (Vicente et al., 2011).

A description of the basic principles of the most common quantitative assessment methods follows, including the capacity spectrum method (CSM), the fragility through capacity spectrum method (FRACAS), the failure mechanism identification and vulnerability evaluation (FaMIVE), the methodology of HAZUS, and the probabilistic post-earthquake functionality assessment method. It is followed by a more detailed description of the qualitative assessment methods prescribed in Canada such as the rapid screening National Research Council (NRC 1992) method and the parametric seismic risk assessment method of CSA S832 (CSA, 2014) for OFCs.

1.2.1 Quantitative assessment methods

1.2.1.1 CSM (Capacity spectrum method) and the use of nonlinear analysis

The capacity spectrum method (CSM) is a performance-based seismic analysis method that can be used for many purposes such as the rapid evaluation of a large number of building structures. It is one of the most commonly used procedures to assess the building behaviour during an earthquake. It is essentially a nonlinear static pushover analysis procedure formally developed by Freeman (Freeman, 1998) but its original concept was introduced for seismic evaluations in the ATC-40 (ATC, 1996) as shown in Figure 1.3 to Figure 1.5. This method includes the following steps: (a) development of pushover curve, (b) conversion of pushover curve to capacity diagram, (c) conversion of elastic response spectrum from standard format to A-D format, and (d) determination of displacement demand. (A: standard pseudo-acceleration, D: Deformation spectrum ordinate).

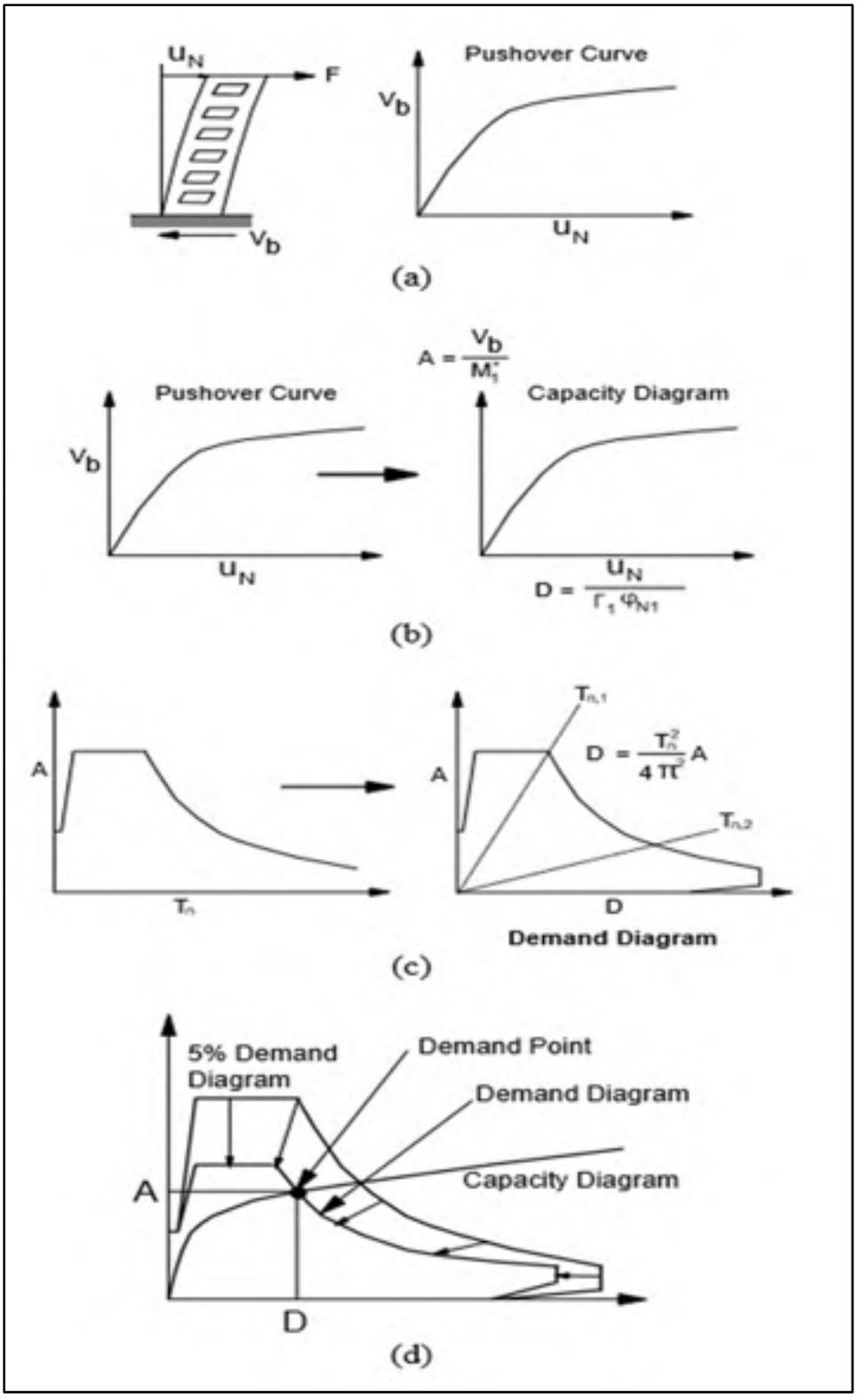

Figure 1.3 Nonlinear static analysis procedure
(Source: ATC (1996))

As shown in Figure 1.3, u_N is the top floor displacement, ϕ_{N1} is the fundamental mode shape ordinate at the top floor, V_b is the base shear and Γ is the modal participation factor and M_1 is the effective modal mass for the fundamental vibration mode. The V_{total} shoin Figure 1.4 is the total lateral load and Δ is the global displacement.

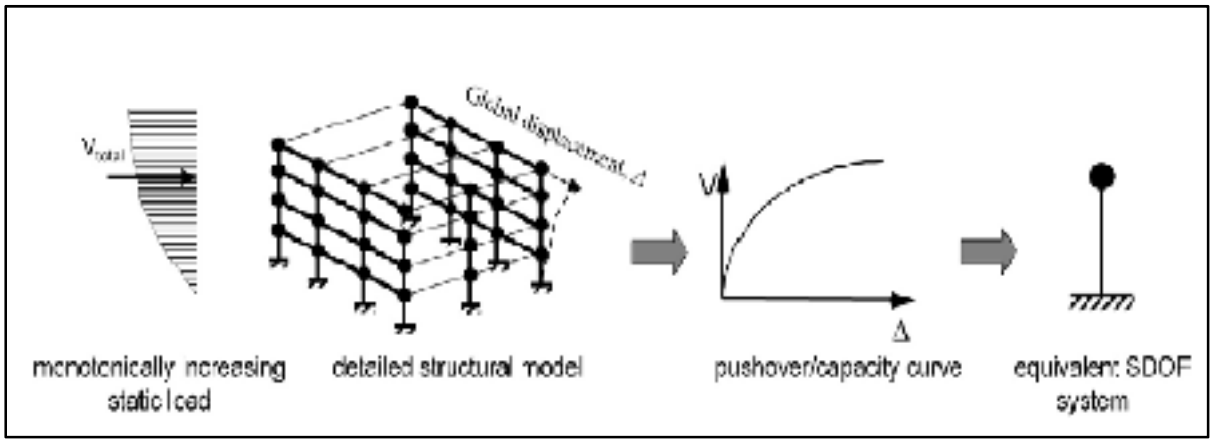

Figure 1.4 Schematic of Static Pushover Analysis used in the Capacity Spectrum Method (Source: ATC (2005))

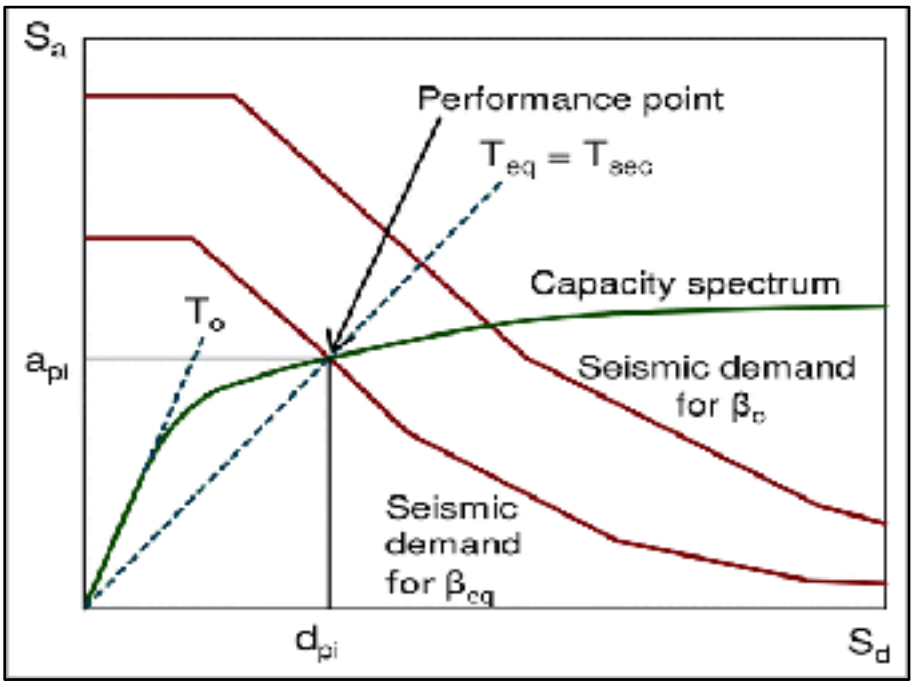

Figure 1.5 Graphical representation of the capacity spectrum method (Source: ATC (2005))

As shown in Figure 1.5, the seismic demand in acceleration, S_a, and relative displacement, S_d, of an equivalent single degree-of-freedom system is represented by a response spectrum (curves in red) and the structural capacity is represented by the pushover curve (in green). This format is called the acceleration-displacement response spectrum (ADRS). The expected performance of the structure, called the performance point, is the intersection point of the seismic demand and capacity spectrum curves. To account for the nonlinear inelastic behavior of the building, a viscous damping ratio β is introduced. Therefore, each building type is modeled as a nonlinear single-degree-of-freedom (SDOF) for which the maximum inelastic deformation is calculated based on the maximum elastic deformation of an equivalent linear elastic SDOF with equivalent fundamental period (T_{eq}) and viscous damping ratio (β_{eq}). Where β_0 shown in Figure 1.6 represents the initial damping value and β_{eq} is referred to as effective viscous damping. The equivalent fundamental period and damping ratio are determined from the seismic demand and capacity curves for a given lateral load resisting system. As mentioned above, the capacity curve is the lateral force-deformation relationship for a given structure obtained from pushover analysis. Therefore, the fundamental period corresponding to the point of intersection of the demand curve and the capacity curve is considered as the equivalent period of the linear SDOF oscillator. The equivalent viscous damping is estimated from the energy dissipated in a vibration cycle of the inelastic system and the equivalent linear system. The estimated spectral displacement is then used to determine the cumulative probability of complete damage from the fragility curves specific to the building type.

In addition to this nonlinear static analysis approach, there is a more exact nonlinear dynamic analysis (NDA) method. In this method, the first step is to create a finite element model of the building structure to capture its nonlinear post-elastic response under ground motions, as shown in Figure 1.6. NDA allows higher modes of vibration to be captured as well as different failure modes, which is not properly done in the ADRS format. Of course, the quality of the NDA method depends directly on the accuracy of the analysis model created to represent the real building.

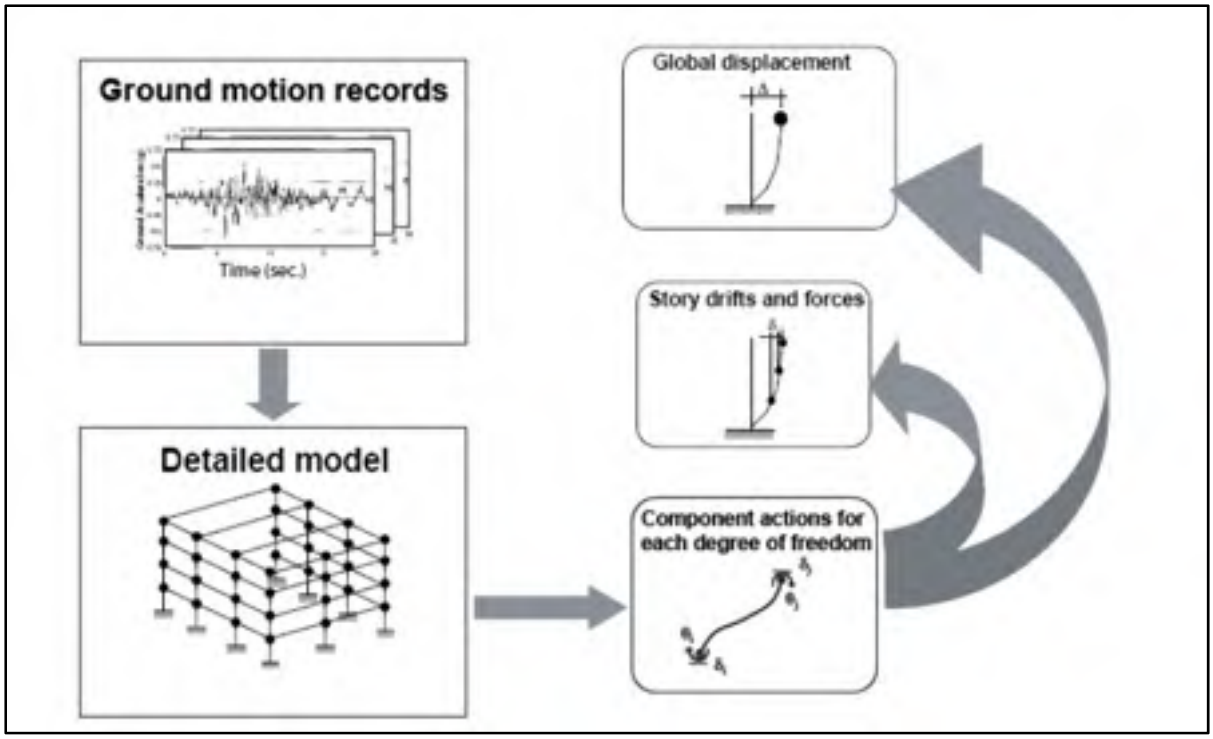

Figure 1.6 Flow Chart of NDA to Determine Seismic Building Response
(Source: ATC (2005))

The nonlinear dynamic procedure is used to represent the seismic response of buildings to several different ground motions for different earthquakes corresponding to tectonic models appropriate for the building location. NDA permits to obtain not only the mean response to a specific ground motion, but it also allows to account for the nonlinear response of buildings generated by different records for the same earthquake intensity measure (Jalayer & Cornell, 2009) (Vamvatsikos & Cornell, 2005), while the linear dynamic procedure ignores the nonlinearity caused by permanent damage and the nonlinear static procedure ignores the inertia effects. Nowadays, the NDA approach is used mostly for design retrofits, but it has the potential to predict the amount of damage and assess the seismic risk.

1.2.1.2 FRACAS (FRAgility through Capacity Spectrum Assessment)

Like NDA, the fragility through capacity spectrum assessment (FRACAS) allows the use of scaled and unscaled ground motions and gives the immediate seismic response of the structure

(Rossetto et al., 2016). This method is more time-consuming than the static approaches (CSM), and its main steps consist of: (a) definition of the idealized trilinear curve that fits the structure capacity curve; (b) identification of Analysis Points (AP), (c) comparison of the elastic demand spectrum with the capacity curve at the performance point (PP) of the demand curve with the line representing the yield period of the structure; (d) determination of the PP , as shown in Figure 1.7. S_a shown is the spectral acceleration, S_d is the spectral displacement, T_y is the yield period, AP is the analysis point and μ is the top floor displacement. Moreover, the blue line represents the structure capacity curve and the green and red lines represent the yield point of the structure.

As illustrated in Figure 1.7, the first step of FRACAS consists of converting the pushover curve to a capacity curve in terms of acceleration-displacement representation, taking into account the floor masses and the inter-story displacement (Figure 1.7a). The second step is dividing the capacity curve into series of checking points with various pre-and post yield points (Figure 1.7b). This step is followed by computing the elastic response from input ground motions (Figure 1.7c). The last step consists of calculating the inelastic demand of the equivalent single degree of freedom for the specified post-yield period (Figure 1.7d). This modified capacity spectrum assessment method is highly efficient to derive fragility curves from dynamic analysis of structures subjected to a series of earthquakes, considering the variability in seismic and structural properties.

Previous studies (Rossetto et al., 2016) have shown that the FRACAS procedure outperforms CSM and its variants, particularly for the cases of low- and mid-rise regular RC frames of various vulnerability classes. This method is recommended in the Guideline Elements Model (GEM) for Analytical Vulnerability Estimation (D'ayala et al., 2014). Further details on the FRACAS methodology are also provided in Gehl et al. (2014). Examples of implementation on RC buildings representative of European and Mediterranean/Italian stocks can be found in Rossetto et al. (2016).

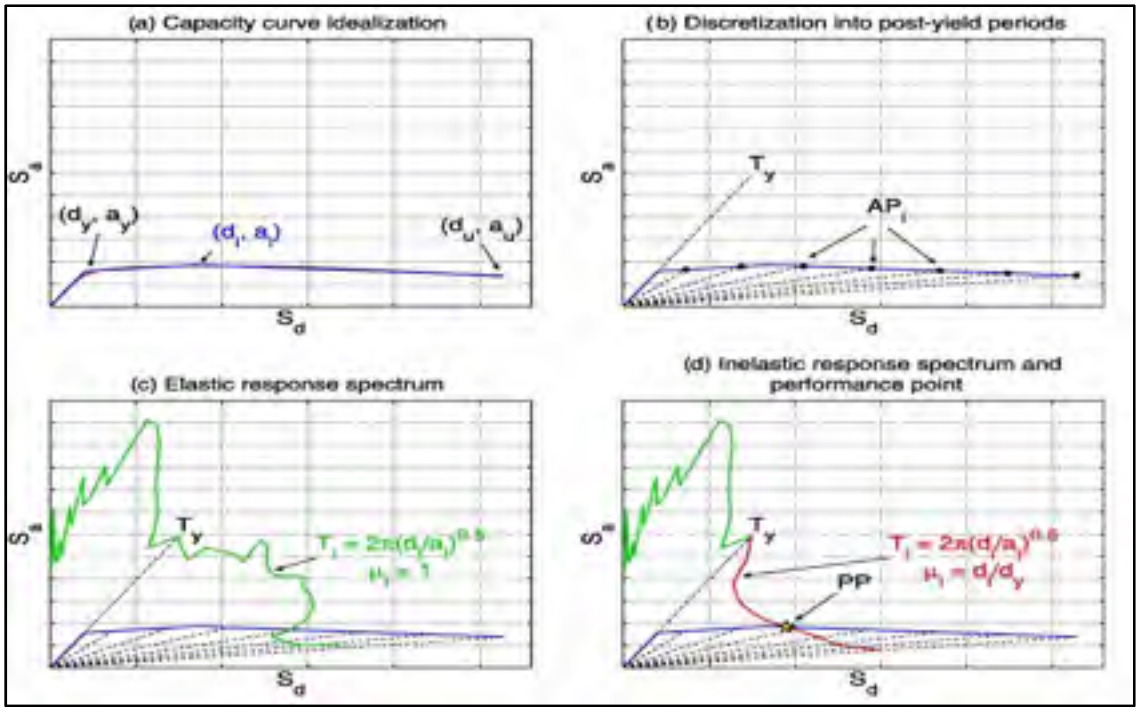

Figure 1.7 Main steps of FRACAS for the derivation of the performance point (PP) using the trilinear idealization model
(Source: Rosetto et al. (2016))

1.2.1.3 FaMIVE (Failure mechanism identification and vulnerability evaluation)

The failure mechanism identification and vulnerability evaluation method, FaMIVE, was developed by D'Ayala and Speranza (D'Ayala & Speranza, 2003). It estimates the seismic performance of the structure in terms of base shear and deformation capacity taking into consideration the collapse mechanisms and determines the fragility functions.

The FaMIVE method was applied to estimate the performance of buildings in several locations worldwide such as Nepal (D'Ayala, 2004), India (D'Ayala & Kansal, 2004), Italy (D'Ayala & Paganoni, 2011) , and in the Casbah of Algiers (Novelli et al., 2015). As done in FRACAS, it also uses a nonlinear pushover analysis to estimate the building performance; the main procedure is shown schematically in Figure 1.8. The main difference between this method and FRACAS is that it provides a specific collapse load factor for each collapse mechanism and it

simulates the performance of buildings needed to derive the corresponding capacity curves. As shown in Figure 1.8, this procedure starts by a detailed inspection and data collection survey of cracks and damage from past earthquake, as well as for the geometric and structural characteristics using a FaMIVE inspection form. The next step is the calculation of the collapse load factor for each façade, either for a part or the whole façade. This step is followed by an equivalent non-linear single degree of freedom to simulate the performance of the building in order to derive the capacity curves to be compared to a spectrum demand curve. Then, the median and the standard deviation of the performance point displacements should be computed in order to derive the fragility curves shown in Figure 1.8 for different limit states. Four limit states are identified: the damage limitation (DL), significant damage (SD), near collapse (NC) or partially collapse and the total collapse (C). Finally, the performance point is derived from the intersection of the capacity curve with the demand spectra for different return periods. The term λ represents the load factor, μ is the ductility factor, M_{eff} is the tributary mass, T_{eff} is the natural period, and K_{eff} is the lateral effective stiffness

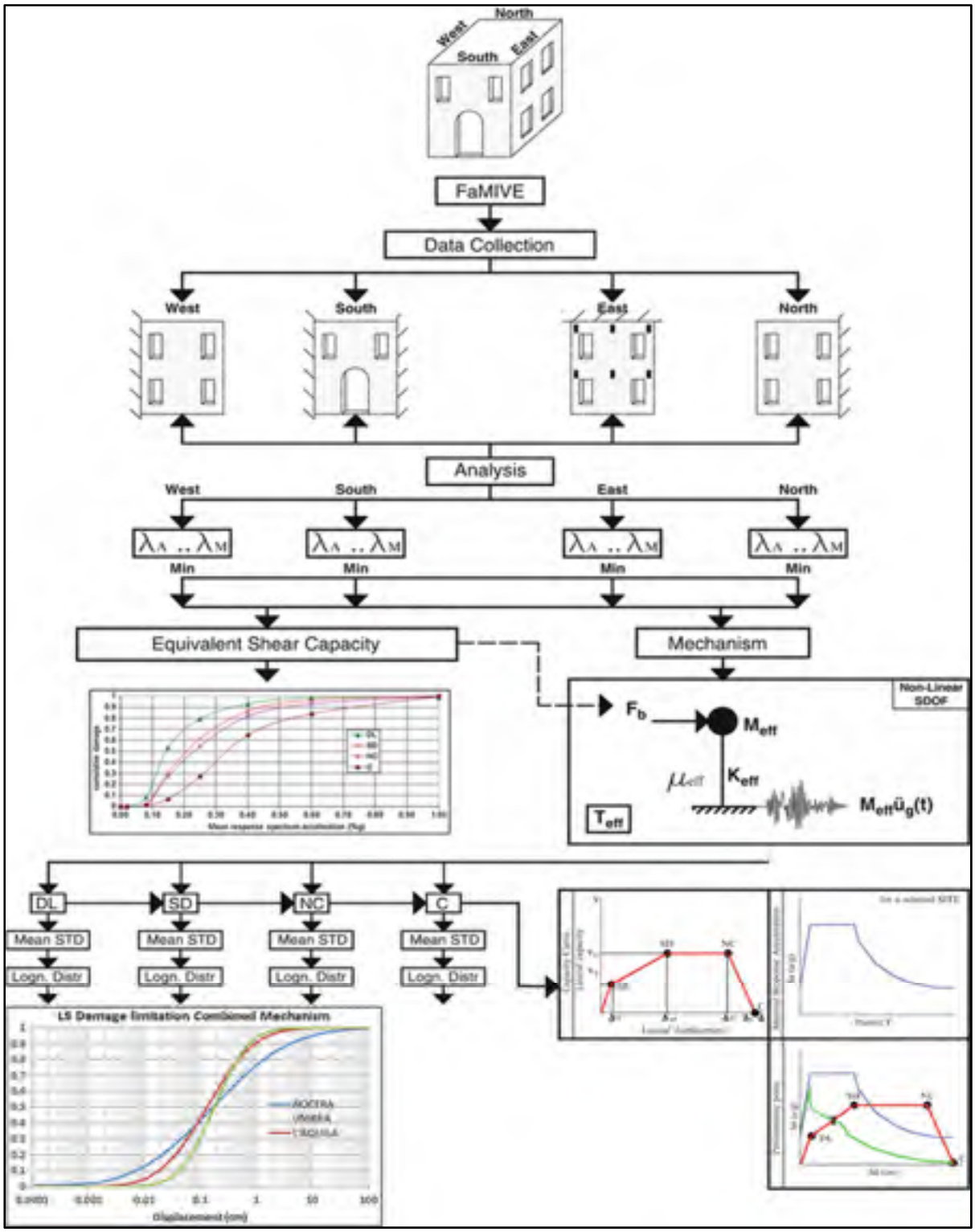

Figure 1.8 Flowchart of the FaMIVE procedure
(Source: D'Ayala and Speranza. (2003))

1.2.1.4 The methodology of Hazard United States (HAZUS) (FEMA454, 2006)

The HAZUS method was developed in the United States by the National Institute of Building Sciences (NIBS) for the Federal Emergency Management Agency (FEMA) (HAZUS-MH, 2004). It is used to assess the seismic risk of buildings, followed by an estimation of the anticipated losses from earthquakes of prescribed magnitudes. The HAZUS methodology and software contains six major modules as shown in Figure 1.9: Potential Earth Science Hazard; Inventory; Direct Damage; Induced Damage; Direct Losses; and Indirect Losses. HAZUS was specifically developed for the estimation of direct and indirect economic and social losses from earthquakes. It combines several elements of risk assessment and is applicable on many levels: inventory databases such as building stock, lifeline systems; state-of-the-art models to relate the magnitude of an event to damage and to estimate the probability of occurrence of a given magnitude event.

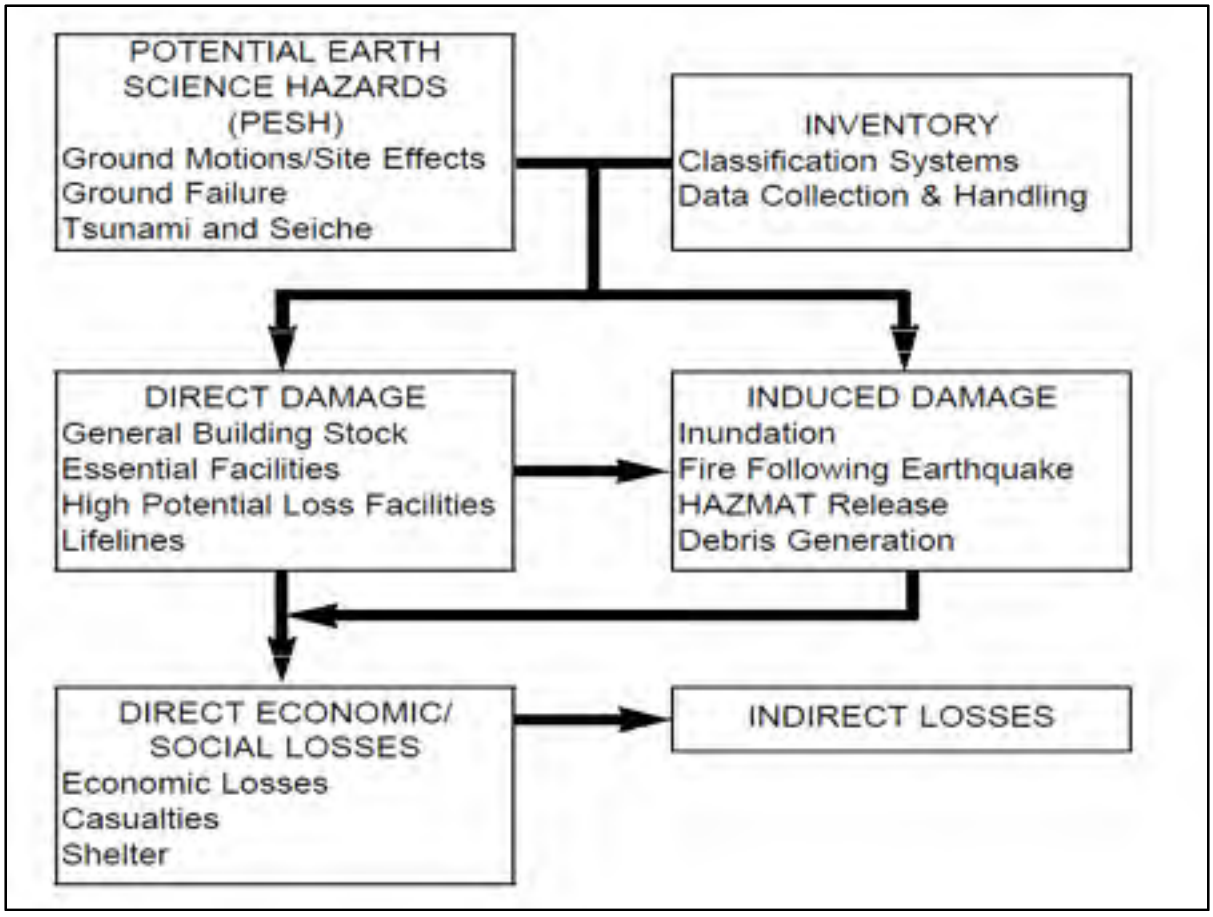

Figure 1.9 Modules of HAZUS
(Source: Kircher et al (2006))

The Potential Earth Science Hazards (PESH) module estimates ground failure and ground motion, based on the fault type and location and the earthquake magnitude selected by the user. For ground failure, the ground deformation and the probability of occurrence are determined based on liquefaction and landslide susceptibility. In addition, other natural hazards such as tsunami or floods can be modeled to assess potential impacts. The inventory module describes the physical infrastructure and demographics of an area. It classifies the infrastructure based on standard classification such as general building stock, essential and high potential loss facilities, components of transportation lifeline systems and components of utility lifeline systems. The direct damage module provides damage estimates in the form of probabilities of exceeding a given level of damage based on a prescribed ground motion according to FEMA 273 (FEMA, 1997) and ATC 40 (ATC, 1996). The induced damage is evaluated as secondary

consequences of the earthquake, such as the consequences of fire or demolition of damaged structures. The direct economic losses module includes the cost of repair and replacement of the damaged buildings and the loss of revenues due to business interruption. The Direct social losses module is further categorized in terms of human casualties and short-term shelter needs.

The HAZUS functions are the capacity curves and the fragility curves. As previously defined for the other methods, the capacity curves serve to determine the probability of damage of the structural elements and for both the drift-sensitive and acceleration-sensitive OFCs. Also, the fragility curves classify the damage into four physical damage states: slight, moderate, extensive and complete, as shown in Figure 1.10; more details about the damage functions can be found in Kircher et al. (1997) and in the software manual users guide (HAZUS, 1999).

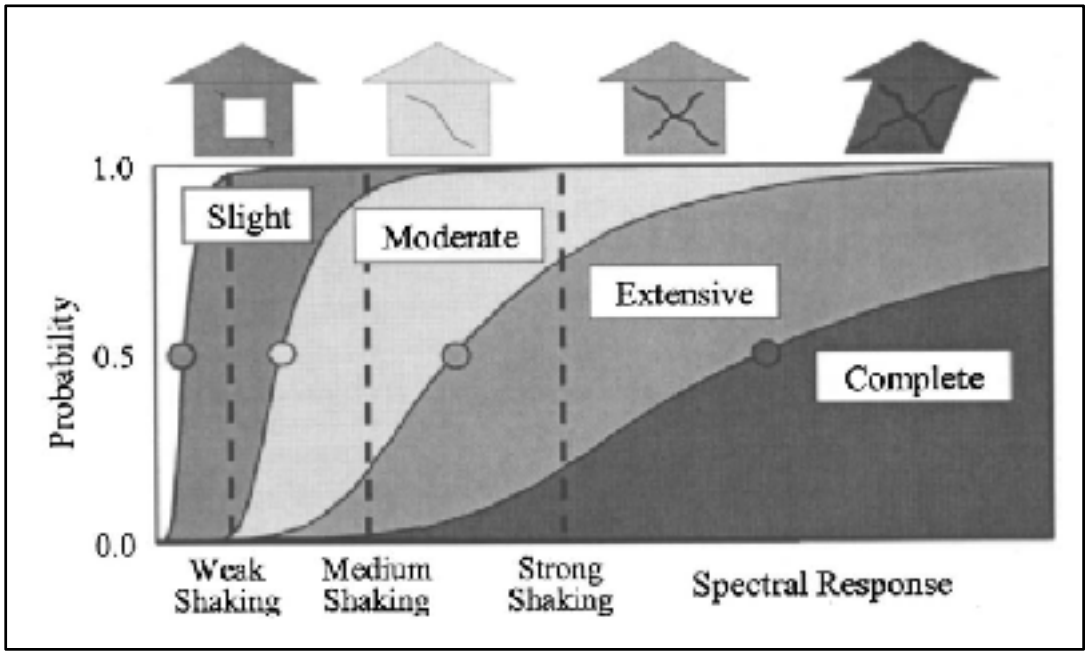

Figure 1.10 Fragility curves for slight, moderate, extensive and complete damage (Source: Kircher et al. (2006))

The capacity curves are derived from pushover analysis for each building type and represent different lateral force resisting systems and building performance levels. These curves are defined by two control points, the yield capacity and the ultimate capacity, as shown in Figure

1.11. The yield capacity represents the elastic lateral strength and the ultimate capacity represents the maximum strength of the building when the structural system collapses as a full mechanism.

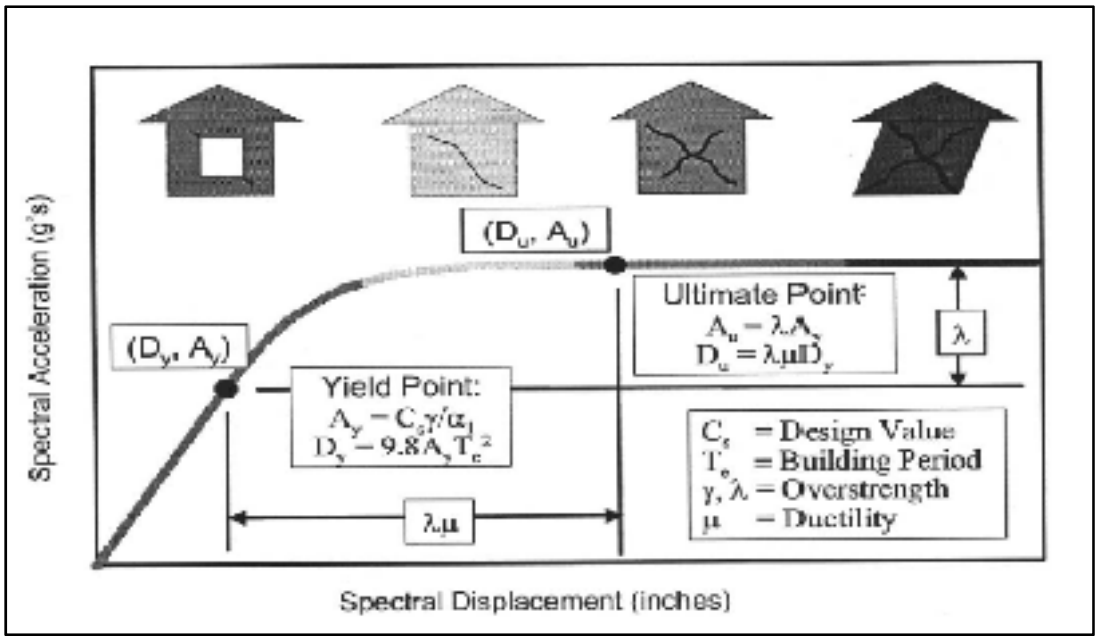

Figure 1.11 Example of a building capacity curve
(Source: Kircher et al. (2006))

1.2.2 Qualitative assessment methods

1.2.2.1 Adapted rapid visual screening method (Tischer, 2012)

The adapted rapid visual screening method is a score assignment procedure proposed by Tischer (Tischer, 2012) to assess the seismic vulnerability of school buildings in Montréal. It is based on the capacity spectrum approach and adopts the same principles as the FEMA 154 method (FEMA454, 2006), with the introduction of the effect of structural irregularities. Therefore, the method considers six parameters: building height, type of lateral load resisting system, construction year, presence of structural irregularities, potential for pounding of

adjacent building(s), and local soil conditions (site classes are according to NBC). This screening method was applied to 101 school buildings designated as post-critical emergency shelters by the City of Montréal.

The seismic structural vulnerability of buildings is represented by an overall score S, which is equal to the summation of the basic structural hazard score (BSH) and various score modifiers related to each of the aforementioned parameters, as indicated in Equation (1.1)

$$S = BSH + \Sigma \text{ (score modifiers)} \quad (1.1)$$

For a given earthquake hazard, the BSH reflects the building performance based on the LLRS type according to FEMA 154. The score modifiers consider other features that make the building more or less vulnerable to seismic damage. The BSH is defined in Equation (1.2) as the negative logarithm of the probability of structural collapse under a specified extreme ground motion, the so-called maximum considered earthquake (MCE).

$$BSH = - \log_{10} [P \text{ (collapse MCE)}] \quad (1.2)$$

The probability of collapse is estimated using the capacity spectrum method and fragility curves corresponding to various lateral load resisting systems (ATC, 2002). The expected seismic behaviour of a building is described by generic capacity curves. As mentioned before, the capacity curves give a relation between the lateral force and sway displacement in the structure and are defined by building type, height and quality of construction (ATC, 2002). The conditional probability of collapse is expressed in Equation (1.3).

$$P \text{ (collapse given MCE)} = p \text{ (complete } | \text{dpi)} \times \text{collapse rate} \quad (1.3)$$

Where p(complete |dpi) is the probability of being in complete damage state given a spectral displacement dpi, and the collapse rate is based on judgment and limited building collapse observations available for each type of LLRS identified in Table 1.1 and it is set to vary

between 0.03 and 0.15. This rate is based on failure modes where either local collapse of a wall or collapse of a single story, without significant ability of total structure collapse. The collapse rate will be greater than 15% if the building is expected to have a high probability of total collapse. Then, the BSH of each LLRS is evaluated based on the probability of collapse. The collapse rates of different building types for complete structural damage are taken from *HAZUS-MH MR4 Technical Manual* (NIBS, 2003) and given in Table 1.2. For more detailed description of the procedure of the determination of the collapse rates, the reader can refer to the *HAZUS-MH MR4 Technical Manual.*

Table 1.1 Types of Lateral Load Resisting Systems according to FEMA 154 (Adapted from ATC (2002))

Type	**FEMA154 Denomination**	**Description**
WLF	W1	Wood light frame
WPB	W2	Wood, post and beam
SMF	S1	Steel Moment Resisting frame
SBF	S2	Steel Braced Frame
SLF	S3	Steel Light frame
SCW	S4	Steel Frame with Concrete Shear walls
SIW	S5	Steel Frame with infill masonry shear wall
CMF	C1	Concrete moment resisting frame
CSW	C2	Concrete shear walls
CIW	C3	Concrete frame with infill masonry shear wall
PCW	PC1	Precast Concrete walls
PCF	PC2	Precast Concrete frame
RML	RM1	Reinforced Masonry bearing walls with wood or metal deck floors
RMC	RM2	Reinforced Masonry bearing walls with concrete diaphragm
URM	URM	Unreinforced masonry bearing walls

Table 1.2 Collapse rates by model building type for complete structural damage

(Adapted from NIBS (2003))

Type OF LLRS	**Probability of collapse (complete damage state)**
WLF	0.03
WPB	0.03
SMF-L	0.08
SMF-M	0.05
SBF-L	0.08
SBF-M	0.05
SLF	0.03
SCW-L	0.08
SCW-M	0.05
SIW-L	0.08
SIW-M	0.05
CMF-L	0.13
CMF-M	0.10
CSW-L	0.13
CSW-M	0.10
CIW-L	0.15
CIW-M	0.13
PCW	0.15
PCF-L	0.15
PCF-M	0.13
RML-L	0.13
RML-M	0.10
RMC-L	0.13
RMC-M	0.10
URM-L	0.15
URM-M	0.15

L: Low rise; M: Medium rise

To calculate the score modifiers, SM, provisional scores are calculated using the same procedure as for the BSH, but the only difference is the input capacity and acceleration spectra. For example, to calculate the score modifier of a given LLRS for a specific soil type, the input acceleration will be according to the soil condition at the building site. Thus, the score modifier is obtained by subtracting the provisional score from the corresponding BSHs as shown in Equation (1.4). The proposed score modifiers are listed in Tables 1.3 and 1.4.

$$SM = BSH - \text{provisional score} \tag{1.4}$$

Table 1.3 Basic score and score modifiers according to Tischer's adapted screening method (Adapted from Tischer (2012))

LLRS	B.M Year	BSH	Mid-Rise	High Rise	Irregularities	
					Vertical	Plan
W1	1970	5.2	0	0	-3.5	-0.5
W2	1970	4.8	0	0	-3	-0.5
S1	1970	3.6	0.4	1.4	-2	-0.5
S2	1970	3.6	0.4	1.4	-2	-0.5
S3	1970	3.8	0	0	0	-0.5
S4	1970	3.6	0.4	1.4	-2	-0.5
S5	1970	3.6	0.4	0.8	-2	-0.5
C1	1970	3	0.2	0.5	-2	-0.5
C2	1970	3.6	0.4	0.8	-2	-0.5
C3	1970	3.2	0.2	0.4	-2	-0.5
PC1	1970	3.2	0.4	0.6	-1.5	-0.5
PC2	1970	3.2	0	0	0	-0.5
RM1	1970	3.6	0.4	0	-2	-0.5
RM2	1970	3.4	0.4	0.4	-1.5	-0.5
URM	1970	3.4	-0.4	0	-1.5	-0.5

Table 1.4 Basic score and score modifiers according to
Tischer's adapted screening method
(Adapted from Tischer (2012))

LLRS	Pre-Code	Post B.M	Soil C	Soil D	Soil E
W1	0	1.6	-0.2	-0.6	-1.2
W2	-0.2	1.6	-0.8	-1.2	-1.8
S1	-0.4	1.4	-0.6	-1	-1.6
S2	-0.4	1.4	-0.8	-1.2	-1.6
S3	-0.4	0	-0.6	-1	-1.6
S4	-0.4	1.2	-0.8	-1.2	-1.6
S5	-0.2	0	-0.8	-1.2	-1.6
C1	-1	1.2	-0.6	-1	-1.6
C2	-0.4	1.6	-0.8	-1.2	-1.6
C3	-1	0	-0.6	-1	-1.6
PC1	-0.4	0	-0.6	-1.2	-1.6
PC2	-0.2	1.8	-0.6	-1	-1.6
RM1	-0.4	2	-0.8	-1.2	-1.6
RM2	-0.4	1.8	-0.6	-1.2	-1.6
URM	-0.4	0	-0.4	-0.8	-1.6

The overall score result of each building represents its structural vulnerability index that is further classified into four levels according to the ranking system of Table 1.5.

Table 1.5 Seismic vulnerability ranking system used in Oregon with FEMA 154 (Adapted from McConnell (2007))

Seismic vulnerability	Probability of collapse under MCE	Index value
Very high	100%	≤ 0.0
High	10% to 100%	0.1 - 1
Moderate	1% to 10%	1.1 – 2
Low	Less than 1%	≥ 2

The score modifiers with their relative BSH presented in Tables 1.3 and 1.4 are those considered in the adapted screening method. For example, the building height has three categories: low rise (2-3 stories), mid-rise (4-6 stories) and high-rise (7 and more). In order to determine the provisional scores for the buildings, the spectral acceleration values used are the same as those for the Basic Structural Hazard score. The year of construction indicates the seismic provisions used in design; therefore, older buildings are expected to behave more poorly than more recent constructions. As per the FEMA method, two significant years are defined in Table 1.6: the Pre-code year, set as 1970 when the first probabilistic seismic zoning maps were introduced in the NBC, and the Benchmark year, 1990, when the ductility requirements were improved significantly, and inelastic behavior of the structures was taken into consideration in the NBC.

Table 1.6 Damage functions for seismic screening in Eastern Canada

Seismicity	Post-Benchmark (1990)		Pre-Code (1970)
Moderate & High	Moderate Code	Low Code	Pre-Code
Low	Low Code	Pre-Code	Pre-Code

The structural irregularities or weaknesses are classified as low or severe. Horizontal irregularities include re-entrant corners, asymmetric stairways, diaphragm discontinuity and asymmetric partition walls. Similarly, vertical irregularities include steps in elevation, the

presence of soft story, sloping terrain and change in lateral load resisting system type. The soil type for a region may be determined from the available micro-zonation maps and geotechnical data. The value of the shear wave velocity can be estimated using the natural frequency and the depth of the sedimentary layer, and the average shear wave velocity up to a depth of 30 m, V_{s30}, can be used to determine the site class as per NBC. The provisional scores are calculated based on amplification of ground motion and the resultant increase in the spectral acceleration values. Table 1.7 lists the amplification factors for each soil type as well as the shear wave velocity for Montréal according to NBC.

Table 1.7 Ground motion amplification factors for Montréal, according to NBC 2015 (Adapted from NRC/IRC (2015))

Soil type	**Description**	**V_{s30}**	**F_a**	**F_b**
A	Hard rock	V_{s30} > 1500m/s	0.776	0.500
B	Rock	760 m/s <V_{s30}≤ 760m/s	0.876	0.640
C	Soft rock and very dense soil	360 m/s <V_{s30}≤ 760m/s	1.000	1.000
D	Stiff soil	180 m/s <V_{s30}≤ 360m/s	1.124	1.36
E	Soft soil	V_{s30}≤ 180m/s	1.172	2.060
F	Poor soil	[a]	[a]	[a]

[a]: site-specific geotechnical investigation required

1.2.2.2 Manual for screening of buildings for seismic investigation, NRC 92 - Canada

Unlike the FEMA 154 (ATC, 2002) screening method, the NRC 92 method considers the vulnerability of operational and functional components. On the other hand, the FEMA 154 methodology is more accurate than NRC 92 in calculating the vulnerability scores because it is based on the capacity spectrum method.

The NRC 92 manual (NRC/IRC, 1992) is based on data collection by visual inspection of the building. This method determines a structural index dependant on five parameters: local seismicity, soil conditions, type of lateral load resisting system, presence of vertical and horizontal irregularities and building importance, in addition to a non-structural index that is function of the sources of non-structural hazards, the soil conditions and building importance. The sum of these two indices (structural and non-structural) provides a final score called the seismic priority index (SPI). According to NRC 92, the priority for seismic mitigation will be classified as a low if the SPI is less than 10 , as moderate if the SPI ranges from 10 to 20 , as high if the SPI ranges from 20 to 30 , and a potentially hazardous situation that requires immediate attention if the SPI score is larger than 30 (NRC/IRC, 1992).

1.2.2.3 CSA S832 - Seismic risk reduction of operational and functional components of buildings

In Canada, the standard CSA S832 “Seismic Risk Reduction of Operational and Functional Components of Buildings” (CSA, 2014) proposes a parametric method to evaluate the seismic risk associated with OFCs. The evaluation of the seismic risk involves the determination of the seismic vulnerability of the OFCs as well as the consequences of their failure. The seismic risk index of the component, R, is the product of the vulnerability index, V, and the consequence of failure index, C (Equation (1.5)).

$$R= V*C \tag{1.5}$$

During an earthquake, the OFCs are subjected to inertial forces, deformation and impact due to their relative motion and possible interaction with other building components. The qualitative vulnerability index is related to the probability of failure of an OFC when the supporting building is subjected to seismic action. The vulnerability index is affected by a number of parameters that have been discussed in Section 1.2. According to Appendix A of CSA S832, the seismic vulnerability of the OFCs is function of their restraint, potential for

pounding and impact, their location and their flexibility. In accordance with the standard, in addition to the aforementioned OFC characteristics, the seismic vulnerability parameters include the effects of the magnitude of the ground motion and the flexibility of the structure. These parameters are weighted based on their relative importance and are used to calculate the vulnerability index, V (Clause 7.5.2.) according to Equation (1.6).

$$V= V_G * V_B* V_E/10 \quad (1.6)$$

V_G is the ground motion characteristics index and is expressed in Equation (1.7) as the product of the spectral response acceleration value for a period of 0.2 s, S_a (0.2), and the acceleration-based site coefficient, F_a, that is defined in Article 4.1.8.4 of the NBC:

$$V_G= F_a S_a (0.2)/1.25. \quad (1.7)$$

V_B is the building characteristics index, related to the flexibility of the structure expressed in terms of the type of the lateral load resisting system, the building fundamental natural period and the soil type, as per Table 1.8 (Clause A.4.4). The minimum and the maximum values of V_B are 1.0 and 1.5, respectively.

Table 1.8 Building characteristics index according to CSA S832-14

	Building fundamental period (s)			**Lateral Load Resisting System (LLRS)**
	0 < T < 0.2s	**0.2s < T < 0.5s**	**0.5s < T**	
Number of stories	1-2	3-4	>5	Steel Moment Resisting Frame
	1-2	3-5	>6	Reinforced Concrete Moment Resisting Frame
	1-2	3-7	>8	Concrete Shear Wall
	1	2-4	>5	Braced Frame
	V_B	**V_B**	**V_B**	**Soil Type**
	1	1.1	1.2	Site Class A: Hard Rock
	1	1.2	1.3	Site Class B: Rock
	1.1	1.2	1.3	Site Class C: Very Dense Soil and soft rock
	1.2	1.3	1.4	Site Class D: Stiff Soil
	1.3	1.4	1.5	Site Class E: Soft Soil
	1.5	1.5	1.5	Site Class F: Sandy Soil

V_E is the OFC characteristic index obtained by the weighted sum of four rating scores according to the Equation (1.8):

$$V_E = \Sigma_{i=1,4} (RS_i * WF_i) \quad (1.8)$$

RS_1 represents the rating score for OFC restraint, RS_2 is the rating score for OFC impact/pounding effects, RS_3 is the rating score for OFC overturning and RS_4 is the rating score for OFC flexibility. The weight factors WF_i associated with each parameter are given in Table 1.9.

Table 1.9 Individual OFC parameters and weight factors according to CSA S832-14

Parameter	Weight Factor
OFC Restraint	4
OFC Impact/Pounding	3
OFC Overturning	2
OFC Location and Flexibility	1

The OFC restraint represents the strength of connections between the OFC and the structural components. The OFC impact and pounding indicates the possibility of impact of the OFC on the other surrounding OFCs and structural components during ground shaking; therefore, an adequate gap should be provided between adjacent OFCs and between the OFCs and the structural components. The OFC vulnerability to overturning is represented by the height of the OFC centre of gravity above the floor level (h) relative to the dimension of its base (d). As per Clause A.4.2.3 of the standard, the maximum horizontal seismic force acting at the OFC centre of mass V_p is calculated according to Equation (1.9).

$$V_p = 1.2F_aS_a\,(0.2)\,W_P \tag{1.9}$$

Where W_P is the weight of the OFC, F_a is the acceleration-based site coefficient and S_a (0.2) is the spectral response acceleration value at a period of 0.2s.

The OFC location and flexibility are represented by the floor level since the acceleration response typically increases with building height, which affects more the OFC located on the rooftop and at upper levels. The rating scores for the OFC vulnerability characteristic index V_E are presented in Table 1.10 as provided in CSA S832.

Table 1.10 Rating scores for OFC characteristic index according to CSA S832-14

Vulnerability Parameters	**Parameter Range**	**Rating Score**	**Weight Factor**
OFC Restraint (RS_1)	Full Restraint	1	4
	Partial Restraint	5	4
	No Restraint	10	4
OFC Impact/Pounding (RS_2)	Gap Adequate	1	3
	Gap Inadequate	10	3
OFC Overturning (RS_3)	Fully Restrained against overturning or		
	$(h/d) \leq 1/(1.2\ F_o\ S_a\ (0.2))$	1	2
	$(h/d) > 1/(1.2\ F_o\ S_a\ (0.2))$	10	2
OFC Flexibility and Location in building (RS_4)	Stiff or Flexible OFC on or below ground floor	1	1
	Stiff OFC above ground floor	5	1
	Flexible OFC above ground floor	10	1

The consequence index, C, is determined from the anticipated consequences of the OFC failure. It is the sum of the rating scores related to life safety (LS), limited functionality (LF), full functionality (FF) and property protection (PP), based on the OFC seismic performance and the impact of its failure or malfunction. Table 1.11 presents the consequence rating scores based on the performance of the OFCs according to the CSA standard.

Table 1.11 Rating scores used for the determination of the consequence index of OFCs according to CSA S832-14

Consequence Parameters	**Parameter Range**	**Rating Score (RS)**
Life Safety (LS)	Threat to very few (N < 1)	1
	Threat to few (1 < N < 10)	5
	Threat to Many (N > 10)	10
Limited Functionality (LF)	OFC breakdown greater than one week is tolerable	0
	OFC breakdown up to 1 week is tolerable	1
	OFC in high importance category building and that is not required to be fully functional	3
	OFC in post-disaster facility and that is not required to be fully functional	5
Full Functionality (FF)	Not Applicable	0
	OFC required to be fully functional	10
Property Protection (PP)	Score may vary from 0 to 10 as determined by the owner / Operator	0-10

As mentioned in Appendix C (Clause C.1) of the CSA standard, the seismic risk is calculated for prioritized mitigation so that for an OFC located in a normal importance category building with a seismic risk index (R) less than or equal to 16, mitigation is not required due to limited benefits of risk reduction. The priority for mitigation should be established after risk assessment based on the determined risk index (R) according to Table 1.12.

Table 1.12 Suggested mitigation priority thresholds according to CSA S832-14

Risk Index	Seismic Risk Level	Mitigation Priority
R < 16	Negligible	Not required
16 < R < 32	Low	Low
32 < R < 64	Moderate	Medium
64 < R < 128	High	High
R > 128	Very high	Very high

1.3 Previous studies on post-earthquake functionality of buildings

The post-earthquake functionality of a building is largely dependent on the survival of its non-structural components as well as the good performance the structural resisting system. For schools designated as post-disaster shelters, loss of functionality could be critical.

In order to assess the post-disaster functionality of residential buildings, a stochastic study was done at the University of Oklahoma, USA (Lin & Wang, 2017b), introducing a building portfolio recovery model (BPRM) to estimate the stochastic recovery of buildings following a hazardous event (Lin & Wang, 2017b). The BPRM contains five functionality states such as the restricted entry (RE), restricted use (RU), re-occupancy (RO), baseline functionality (BF), and full functionality (FF). These states are defined as the performance index of a building, which is modeled using discrete-state representing a portfolio-level recovery by computing the building level restoration in temporal and spatial dimensions, using continuous-time Markov Chains (CTMC). Figure 1.12 represents this analysis procedure.

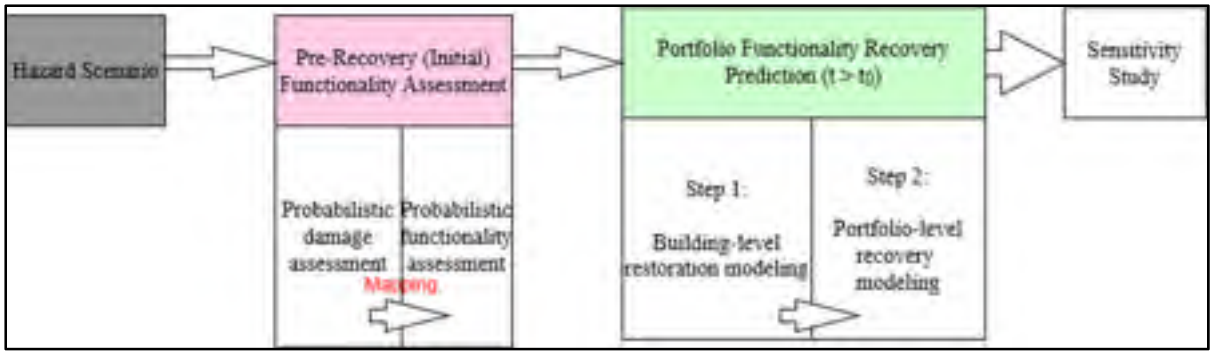

Figure 1.12 Analysis procedure in the building portfolio recovery model (BPRM)
(Source: Lin & Wang (2017b))

The first step in the building portfolio recovery method is the pre-recovery (initial) functionality status immediately at the time of occurrence of the earthquake (t_0). This step involves the assessment of the initial functionality state before the beginning of any recovery activity. That type of assessment is usually done by engineers according to the ATC-20 (Oaks, 1990) and the functionality losses need to be estimated according to a probabilistic approach as shown in Figure 1.13.

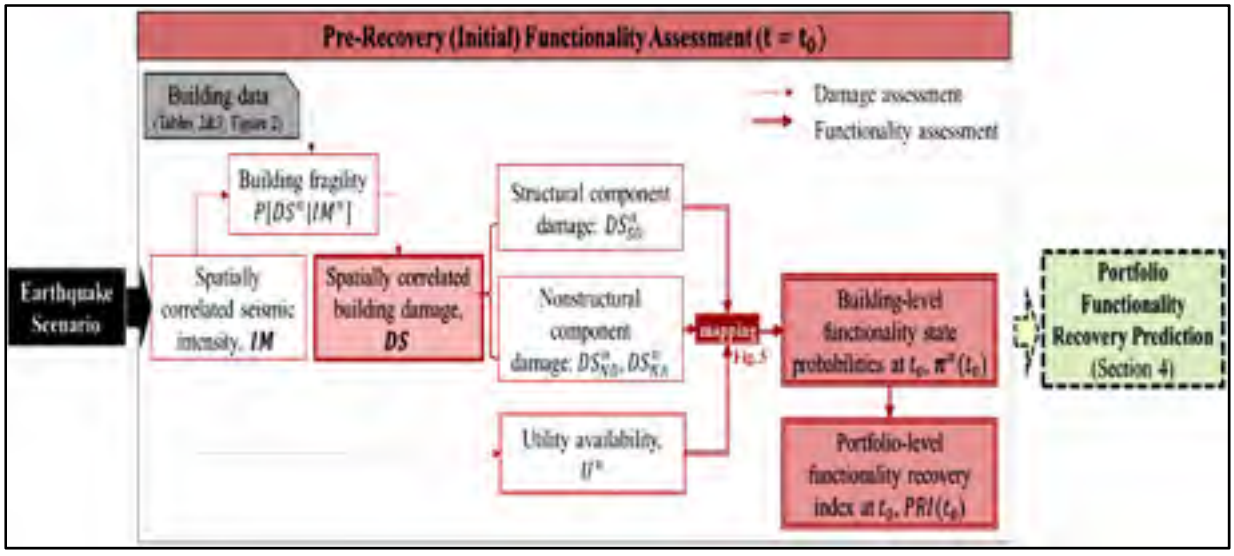

Figure 1.13 Flowchart of the probabilistic approach of pre-recovery damage and functionality loss assessment
(Source: Lin & Wand (2017b))

As shown in Figure 1.13, the probabilistic approach proceeds by estimating the damage of the structural components (DS_{SD}^{n}) and of both the drift-sensitive (DS_{ND}^{n}) and the acceleration-sensitive (DS_{NA}^{n}) non-structural components for a given earthquake scenario. Mapping or overlaying the structural component damage state and the non-structural component damage states with the availability of utility service of the building, U^n, will result in the building-level functionality state probabilities and the portfolio-level functionality recovery index, PRI, as a function of t_0. The second step following the pre-recovery functionality assessment is the building portfolio functionality recovery prediction for a period of time larger than t_0 ($t > t_0$). Based on the pre-recovery step, a recovery analysis is conducted to estimate the building-level restoration functions (BRF) and portfolio-level recovery trajectory, $PRI_j(t)$, and the recovery time $PRT_{FF,95\%}$ which is the time needed to restore 95% of the building to full functionality (Lin & Wang, 2017a). The BPRM can be summarized in Figure 1.14.

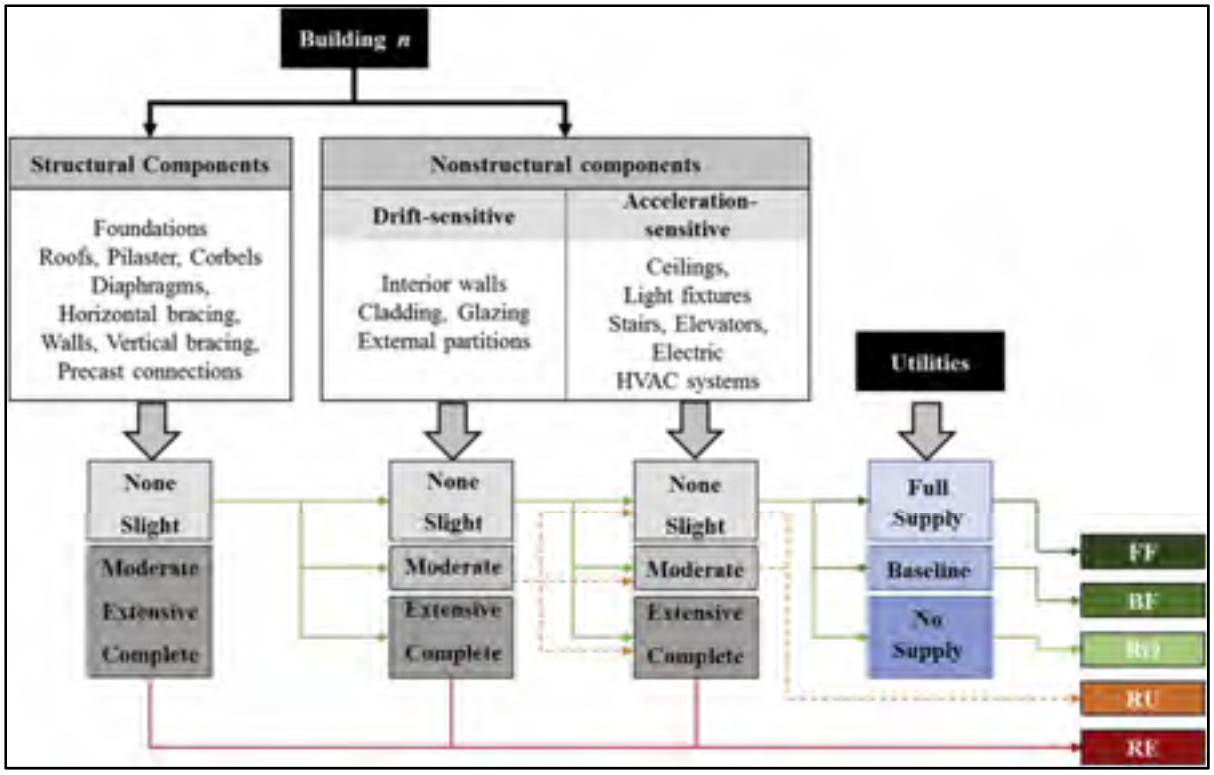

Figure 1.14 Building damage and utility availability to building functionality states (Source: Lin & Wang (2017a))

1.4 Previous studies on the effects of soil-structure resonance

The soil-structure resonance phenomenon is an important aspect of the dynamic behavior of a structure subjected to a ground motion. Resonance amplifies the seismic response of the building and leads to potential structural and non-structural damage, especially if internal structural damping is low. It may also lead to soil liquefaction in vulnerable sites (Soil Class E). Resonance will occur when the site period and the fundamental period of the building are close to each other (Bolander et al., 2001). Figure 1.15 shows a schematic graph of the amplification of building accelerations due to soil-structure resonance.

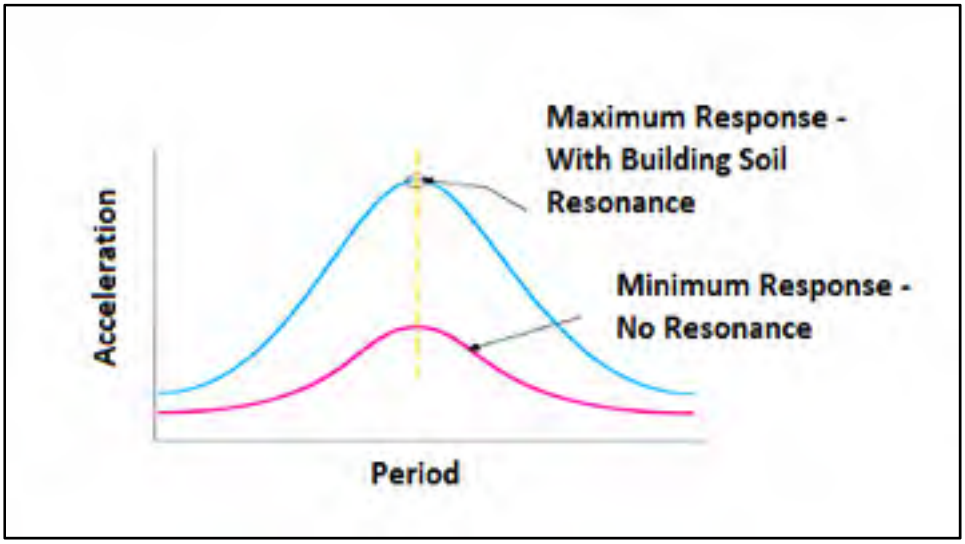

Figure 1.15 Effect of resonance on the seismic response of buildings
(Source: FEMA454 (2006))

As larger lateral inertia forces are induced at resonance, soil-structure resonance can strongly increase the building deformations (Kvasnicka et al., 2011) and damage to drift-sensitive OFCs.

Mucciarelli et al. (2004) have analyzed the effect of soil-building resonance and the elongation of the fundamental period of the structure due to stiffness reduction induced by structural damage after the successive October 31 M_w 5.4 and November 1, 2002 M_w 5.3 earthquakes

that occurred at the border between Molise and Puglia in Southern Italy. To test if the soil-building resonance had increased the structural damage, ambient vibration data were recorded inside the most damaged building after the first earthquake, then during and after the second one. The recorded data were analyzed to estimate the fundamental frequency of the building and its shift (period elongation) due to damage. The analysis was done using many techniques such as the Short-Time Fourier Transform (STFT), Wavelet Transform (WT), Horizontal-to-Vertical Spectral Ratio (HVSR) and the Horizontal-to-Vertical Moving Window Ratio (HVMWR). To estimate the fundamental frequency of the soil supporting the building, three different techniques were applied such as noise HVSR, Strong motion HVSR of seven aftershocks, and 1-D modeling (soil column) based on a velocity profile derived from noise analysis of surface waves (NASW). The different measurements led to the conclusion that the fundamental frequency of the most damaged building is in the same range as the fundamental frequency of the underlying soft sediments before the damage, thus proving that soil-building resonance effects had occurred during the earthquakes.

During the assessment of the seismic vulnerability of school buildings in Tehran City, Iran, Panahi et al. (2014) also considered the seismic resonance coefficient as a main factor affecting the structural vulnerability. Therefore, the resonance coefficient was simply taken as the ratio of the fundamental period of the structure to that of the soil underneath.

Tezcan et al. (2012) concluded that the main reason for the collapse of the Paint Workshop of the Tofas-Fiat automobile factory building in Bursa during the 1970 M_w 7.2 Turkish earthquake was due to soil-structure resonance effects.

As can be concluded from previous studies and observations in past earthquakes, coincidence of the natural period of the structure and that of the supporting soil will lead to significant response amplification that results in increased damage and even collapse. Therefore, during this study it is deemed very important to check the potential for soil-structure resonance.

1.5 Analytical Hierarchy Process (AHP)

The Analytical Hierarchy Process introduced by Saaty (1977) can be used in a wide variety of decision-making processes such as in business, insurance, industry and education. AHP is one of the most commonly used multi-criteria decision-making methods, and is based on the calculation of the relative importance of each parameter affecting the main goal of the study via a pairwise comparison. Then, it transforms the comparison into numerical values that are further processed in a mathematical matrix format. Note that the compared parameters are statically independent, which means that while comparing two parameters affecting the structural vulnerability the other parameters won't affect this comparison. The relative importance of the parameters is identified by assigning a weight factor to each of them based on the scale of preference between each pair of parameters as shown in Table 1.13.

Table 1.13 AHP scale of preference between two parameters
Adapted from Saaty (2006)

Intensity of importance	**Degree of preference**	**Explanation**
1	Equally	Two factors contribute equally to the objective
3	Moderately	Experience and judgment slightly to moderately favor one factor over another
5	Strongly	Experience and judgment strongly or essentially favor one factor over another
7	Very strongly	Experience and judgment strongly or essentially favor one factor over another
9	Extremely	The evidence of favoring one factor over another is of the highest degree possible
2,4,6,8	Intermediate	Used to represent compromises between the preferences in weights 1,3,5,7 and 9
Reciprocals	Opposites	Used for inverse comparison

The important feature of the AHP method is its consistency for weighting the factors. The consistency index (CI) is defined in Equation (1.10)

$$\mathrm{CI} = \frac{\lambda_{max-N}}{N-1} \tag{1.10}$$

Where λ max is the largest or principal eigenvalue of the pairwise comparison matrix of order N. The average random consistency index (RCI) is calculated as shown in Table 1.14 and the consistency ratio CR is obtained from Equation (1.11).

$$CR = \frac{CI}{RI}. \tag{1.11}$$

If CR is equal to zero (i.e. CI = 0), the comparison is completely consistent. If CR is larger than 0.1, the comparison is not consistent, and the pairwise comparison and weighting of the different parameters must be repeated. The random consistency indices presented in Table 1.14 are obtained by the computation of the mean random consistency index (MRCI) based on simulations using a large number of samples ranging from 4600 to 470000 (Tummala & Ling, 1998).

Table 1.14 AHP random consistency indices (RI)
Adapted from Saaty (2006)

N	1	2	3	4	5	6	7	8	9	10	11	12
RI	0	0	0.58	0.9	1.12	1.24	1.32	1.41	1.5	1.49	2	1.5

The random consistency indices presented in Table 1.14 were estimated by several authors that have computed and obtained a mean random consistency index MRCI (N) for matrices of order N (Noble & Sanchez, 1993; Saaty, 2000; Tummala & Ling, 1998; Tummala & Wan, 1994). To compute the MRCIs, Saaty and Uppuluri (1998) have used a computational procedure called Saaty's Eigenvector Method (SEM) while other authors (Tummala & Wan, 1994) have used the Power Method (PM). More details about SEM and PM can be found in Tummala & Ling (1998) and Tummala & Wan (1994).

Conclusion

The review of literature showed that the seismic risk assessment of OFCs computed according the CSA S832-14 standard can be improved by adding new parameters affecting the structural vulnerability, namely the effect of soil-building resonance, the year of construction and the presence of structural irregularities. The integration of these parameters into the structural vulnerability assessment will be conducted using the AHP tool. Moreover, the adapted seismic

screening method developed by Tischer (2012) has considered most of the structural parameters contributing to the seismic structural vulnerability without the possible soil-building resonance effect. To this end, the AHP method is also applied to introduce a coefficient of soil-building resonance in the building vulnerability assessment, thus determining a new improved vulnerability index, as will be detailed in the next chapters.

CHAPTER 2

SEISMIC STRUCTURAL VULNERABILITY OF SCHOOLS IN MONTRÉAL CONSIDERING THE EFFECT OF SOIL-BUILDING RESONANCE

In order to evaluate the soil-building resonance effects as a parameter contributing to the seismic structural vulnerability of schools, a new equation for the vulnerability index, VI, needs to be synthetized as described next, using the AHP approach. The first step is the extraction of the dynamic properties of buildings such as their fundamental frequency and the damping ratio of the corresponding mode from AVM records: this was done first by Tischer (Tischer et al., 2012) for 69 school buildings using the operational modal analysis software ARTeMIS (A/S, 2010). The extracted properties were later validated during this study, using the software Sensequake – 3D SAM (Sensquake, 2017). Since AVM measurements were also taken at the building sites at ground level, the fundamental frequency of the soil was extracted using the Grilla software (Micromed, 2011), and the coefficient of soil-building resonance was obtained by simply dividing the fundamental frequency of the underlying soil by the fundamental frequency of the building.

An equation representing the structural vulnerability without taking into consideration the soil-building resonance was developed and validated through the adapted screening method (Tischer et al., 2012), while another new equation was developed taking into account the contribution of the soil-building resonance ratio. The vulnerability indices were calculated from these two equations using the scores shown in Tables 1.3 and 1.4 and the coefficient of resonance was introduced in the new structural vulnerability equation as a negative value since resonance is adversely affecting the basic score. The final step consisted of scaling the new structural vulnerability index to classify the vulnerability of each school building. In this chapter, the calculation method is described in detail along with the school building characteristics. Finally, a discussion of the reliability of AVM for predicting the modal properties of the underlying soil is presented.

2.1 School building databases

A wealth of information was collected by Tischer as part of her PhD work on rapid seismic screening of sixteen school complexes designated as post-disaster shelters in Montréal (Tischer, 2012). A total of 101 individual buildings were surveyed, which form the database of the current study. In terms of their lateral load resisting systems (LLRS), almost 80% of the school buildings have concrete frames with infill masonry shear walls, concrete shear walls and steel moment frames, as shown in Figure 2.1.

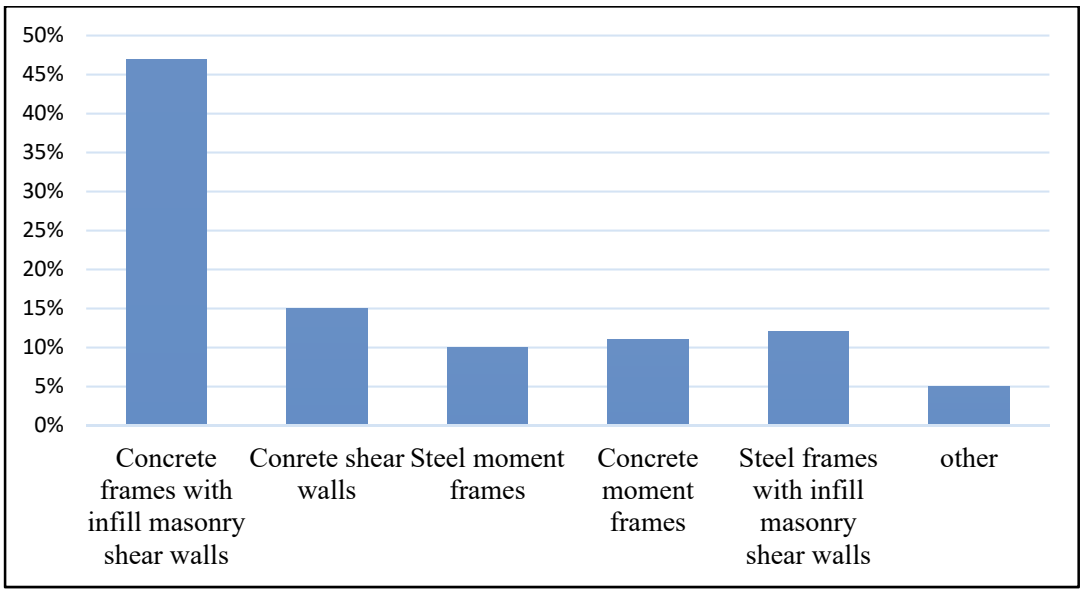

Figure 2.1 Distribution of LLRS for the evaluated schools using the adapted seismic screening method (Adapted from Tischer (2012))

As much as 87% of the surveyed school buildings were constructed during the 1960s and 1970s, thus designed with pre-Code seismic provisions. The building height distribution is represented by the number of floors. Most of the schools are low-rise: 85% of them are three stories or less and the tallest one is six-story high. 80% of the buildings have some form of structural irregularity as defined in the NBC (NRC/IRC, 2015) and 40% combine at least one vertical and one planar irregularity.

2.2 Reliability of the ambient vibration measurement test results

The reliability of the ambient vibration measurements method was also evaluated in this study. Several measurements were performed at a chosen site for seven days and different weather conditions. The site is near the École de technologie supérieure student residence located at 311 Peel Street in Montréal. The measurements were done using a micrometer Micromed Tromino shown in Figure 2.2.

Figure 2.2 Tromino sensor

The recorded AVM data from the Tromino sensor were analyzed using the Grilla software (Micromed, 2011) in order to determine the fundamental frequency of the underlying soil using the H/V technique (Nakamura, 2010). In this research, four measurements were conducted daily at the site for 7 days. Based on the different results extracted with Grilla, the average estimated fundamental frequency of the soil was 4.5 Hz (peak value shown in Figure 2.3) with a calculated standard deviation (Std) of 0.09 using 28 samples. The Std value has increased to 0.19 when the measurements were done during windy days.

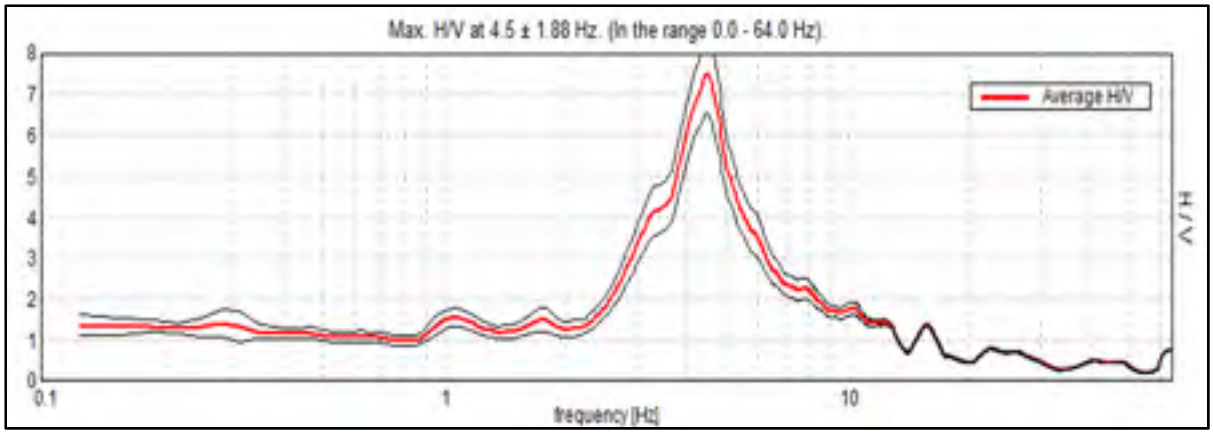

Figure 2.3 Average fundamental frequency of the tested soil site

The peak frequency value of 4.5 Hz in Figure 2.3 also confirms a class-C soil by matching the V_{s30} corresponding to a soil type C according to the NBC and the micro-zonation map of Montréal. Using Equation (2.1) proposed by Chouinard & Rosset (2011), the V_{s30} of the studied site is equal to 378 m/s which is between 360 m/s and 760 m/s, which correspond to soil type C according to Table 1.7. .

$$V_{s30} = 177 + 44.7F_0 +/-89\ m/s \tag{2.1}$$

Where F_0 is the fundamental frequency, V_{s30} is the shear wave velocity at 30m depth.

2.3 Coefficient of soil-building resonance

As mentioned before, the in situ dynamic properties of the school buildings were determined using ambient vibration measurements (AVM) during the previous study at McGill University (Tischer, 2012). The local site conditions were also estimated by in situ AVM tests from which the fundamental natural frequency of the soil was extracted. The coefficient of soil-building

resonance, (CoR), was simply obtained by dividing the fundamental frequency of the school building by the fundamental frequency of the adjacent soil.

The CoR values (see Figure 2.4) show that 16 school buildings out of 69 for which local soil AVM measurements were available are in the range of possible soil-structure resonance, representing 23% of the 69 buildings considered. These results also indicate that 16 of these 16 prone to soil-structure resonance are built on site classes D (8) and E (8), with relatively poor soil conditions.

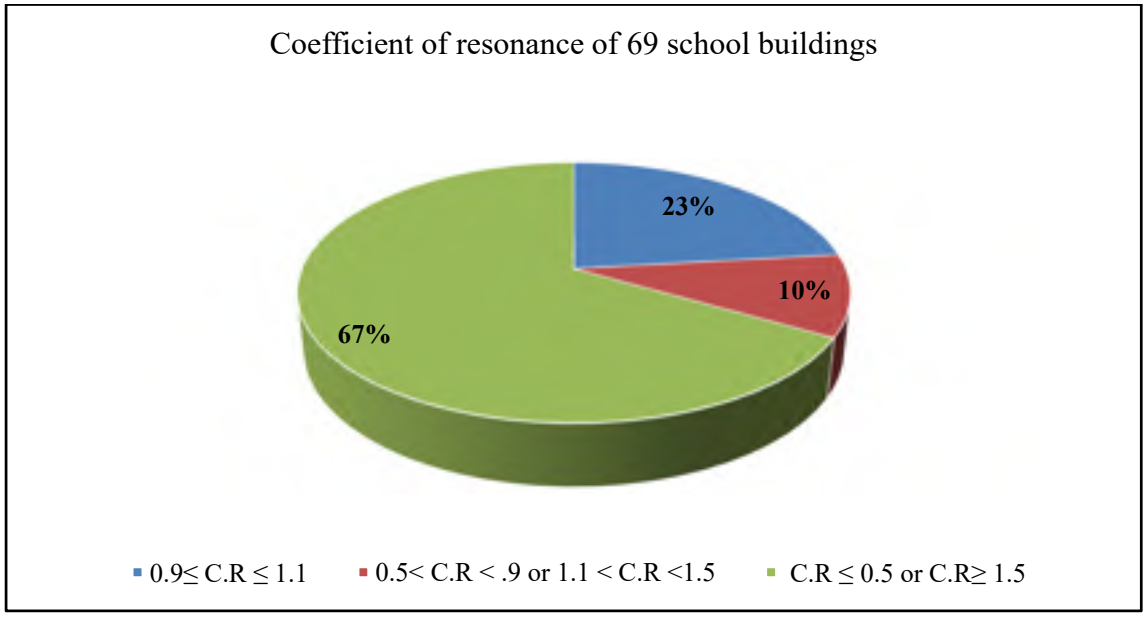

Figure 2.4 Distribution of coefficients of soil-building resonance for 69 buildings located in Montréal

In the absence of equipment to perform AVM, the coefficient of soil-building resonance can be estimated using a microzonation map in order to find the soil type and its fundamental frequency. This can be achieved by entering the latitude and longitude of a studied building in a software called ArcGIS, some microzonation databases could give the geotechnical profile of the location. Moreover, the fundamental frequency of the building, can be estimated using the equations provided in NBC for different types of LLRS.

2.4 Vulnerability index from AHP

The first step in applying the AHP approach is to proceed to the pairwise comparison between the parameters such as the lateral load resisting system, the year of construction, the type of soil (site class), the building height, the presence of structural irregularities and the coefficient of resonance. The comparison is done according to Saaty's scale and translates into the two matrices shown in Tables 2.1 and 2.2 that are used to calculate the weight factor of each parameter. The sum of the weights (last column in the tables) is equal to 1, as each weight represents the percentage of the contribution of each parameter to the total structural vulnerability of a building. As indicated previously, AHP was first applied without taking into consideration the coefficient of resonance, so that the first matrix (Table 2.1) is of order 5. The second matrix (Table 2.2) is also of order 5 but it includes the coefficient of soil-building resonance (P_5) replacing the local soil condition at the site (P_3 in Table 2.1).
One has to recognize that there is some subjectivity in the selection of the priority indices during the pairwise comparison, and this is where expert opinions may be collected for a more robust model. However, in this study, the indices were determined by the author only.

The weight factors obtained in Table 2.2 indicate that the coefficient of soil-building resonance has the highest contribution (31%) among the five parameters. These results are contrasted to those presented in Table 2.1 where the LLRS type is dominant (31%), which is consistent with the fact that the BSH is the highest score of the sum in Equation (1.1) and directly represents the influence of the LLRS type. The consistency ratio for the results in Tables 2.1 and 2.2 is equal to 0.09, which is less then 0.1 (10%)

Table 2.1 Priority and normalized weights of five parameters from the adapted screening method according to AHP

	P_1	P_2	P_3	P_4	P_5	Priority	Weight
P_1 LLRS	1.00	2.00	2.00	1.00	3.00	1.64	0.31
P_2 Year of construction	0.50	1.00	0.50	0.33	2.00	0.70	0.13
P_3 Local soil	0.50	2.00	1.00	0.50	1.00	0.87	0.16
P_4 Irregularities	1.00	3.00	2.00	1.00	1.00	1.43	0.27
P_5 Building height	0.33	0.50	1.00	1.00	1.00	0.70	0.13

Table 2.2 Priority and normalized weights of five parameters including the coefficient of resonance according to AHP

	Parameters	P_1	P_2	P_3	P_4	P_5	Priority	Weight
P_1	**LLRS**	1.00	2.00	1.00	3.00	0.50	1.25	0.23
P_2	**Year of construction**	0.50	1.00	0.33	2.00	0.33	0.64	0.12
P_3	**Irregularities**	1.00	3.00	1.00	1.00	0.50	1.08	0.20
P_4	**Height of building**	0.33	0.5	1.00	1.00	1.00	0.70	0.13
P_5	**Coefficient of Resonance**	2.00	3.00	2.00	1.00	1.00	1.64	0.31

The parameter P_5 shown in Table 2.2 represents the coefficient of resonance, $T_{building}/T_{soil}$.

Using the Priority scores and the weight factors of the last two columns in Tables 2.1 and 2.2, the VI index of each school building of the database is calculated according to Equation (2.2).

$$VI = a * b * c * d * \sum \boldsymbol{X_i} * P_i \tag{2.2}$$

Where X_i is the weight of the parameters resulting from the AHP, and P_i represents the parameter score. The coefficients a to c vary with the type of LLRS: a is equal to 1.2 for steel moment frames (with $b = c = 1.0$), b is equal to 1.3 for steel braced frames (with $a = c = 1.0$) , and c is equal to 1.3 (with $a = b = 1.0$) for concrete shear walls. The coefficient d is equal to

0.8 if the local soil is of class E, or 1.0 otherwise. These coefficients were calculated in order to calibrate the new VI so that if the same parameters are used, the same level of vulnerability will result when compared to Tischer's adapted screening method.

The resulting vulnerability index is evaluated according to a new scale corresponding to Equation (2.2), as defined in Table 2.3. It should be noted that the developed equation of the vulnerability index is specifically applied to the schools of the database, all located on the Island of Montréal where seismic hazard is considered moderate as per NBC.

Table 2.3 Structural vulnerability classes according to the proposed method

Seismic vulnerability	VI Index	Mitigation
Very high	0 – 0.2	High priority
High	0.2 – 0.45	Necessary
Moderate	0.45 – 0.75	Optional
Low	>0.75	Not necessary

2.5 Validation of vulnerability index using AHP

The seismic vulnerability classes of school buildings were evaluated according to the AHP-based equation, first without the coefficient of soil-structure resonance, and then by considering it. The obtained results without the CoR indicated that the seismic vulnerability classes were conforming to those found according to Tischer's adapted seismic screening method (Tischer, 2012). As an example, the structural vulnerability classes of a given school (School 16 in Appendix 1) comprising eight concrete shear wall buildings are shown in Table 2.5. The characteristics of these eight buildings are given in Table 2.4. A detailed calculation of the vulnerability index using the adapted screening method and the AHP based method is given in Appendix IV.

The results from the new scoring procedure without the effect of soil-building resonance show that 97% of the assessed school buildings have the same vulnerability class as obtained from the adapted screening method (results shown in Appendix III). Moreover, the dynamic properties such as the fundamental frequencies of the buildings and the adjacent soil are presented in Appendix II.

Table 2.4 Characteristics of eight concrete buildings (School 16 in Appendix I)

Building	**Building frequency (Hz)**	**Year of Construction**	**Irregularities**		**Soil**	**Frequency from AVM (Hz)**	**Height of building**
			Plan	**Vertical**			
T	3.56	1969	yes	yes	E	3.72	Mid rise
U	3.38	1969	No	yes	E	3.72	Mid rise
V	3.45	1969	No	No	E	3.72	Mid rise
W	3.46	1969	No	No	E	3.72	Mid rise
X	3.63	1969	yes	yes	E	3.72	Mid rise
Y	6.49	1969	No	No	E	3.72	Low rise
Z	3.70	1969	No	No	E	3.72	Low rise
S	4.32	1974	yes	No	E	3.72	Low rise

Table 2.5 Comparison of structural vulnerability indices and classes according to the AHP-based method and Tischer's adapted screening method without the coefficient of resonance

Building	**VI (AHP)**	**Vulnerability Class**	**VI (Adapted screening method)**	**Vulnerability Class**
T	0.2	Very high	-0.1	Very high
U	-0.11	Very high	-0.1	Very high
V	0.79	Low	2.4	Low
W	0.79	Low	2.4	Low
X	0.21	Very high	-0.1	Very high
Y	0.77	Low	2	Low
Z	0.77	Low	2	Low
S	0.84	Low	3.1	Low

When potential soil-structure resonance was considered in the assessment, the results shown in Table 2.6 for these same buildings, all founded on poor soil conditions – Class E, indicate that the vulnerability classes changed considerably, especially for the buildings with a CoR ratio close to 1. For example, building V has a coefficient of resonance equal to 1.08 and the vulnerability index from Equation (2.2) dropped from 0.79 to 0.11, which means that the vulnerability class has increased from low to very high. For buildings Y and S, the vulnerability class did not change since their coefficient of resonance is far from 1. Moreover, as indicated previously, 26% of the studied school buildings were found to have a very high vulnerability class because they are in the range of soil-structure resonance. In such case, a more detailed investigation considering the structural and soil properties should be undertaken to confirm the resulting high vulnerability classes and assessing the need for mitigation.

Table 2.6 Comparison of structural vulnerability index and class according to the AHP-based method with consideration of the coefficient of soil-building resonance for a school campus with 8 buildings

Building	Coefficient of resonance	Analytical equation results (AHP)	Vulnerability Class	VI (Adapted screening method)	Vulnerability Class
T	1.04	-0.06	Very high	-0.7	Very high
U	1.10	-0.38	Very high	-0.1	Very high
V	1.08	0.11	Very High	2.4	Low
W	1.08	0.11	Very High	2.4	Low
X	1.04	-0.04	Very high	-0.1	Very high
Y	0.56	0.77	Low	2.0	Low
Z	1.00	0.16	Very High	2.0	Low
S	0.82	0.84	Low	3.1	Low

The structural vulnerability indices and classes considering the effect of possible soil-building resonance were computed for 14 buildings having a coefficient of resonance between 0.9 and

1.1, and were then compared to the results obtained from the Tischers's adapted screening method as shown in Tables 2.7 and 2.8.

Table 2.7 Comparison of Structural vulnerability index and class according to the AHP-based method considering soil-building resonance and Tischer's adapted screening method for two buildings (School 1 in Appendix I)

Building	Coefficient of resonance	Analytical equation results (AHP)	Vulnerability Class	Adapted screening method	Vulnerability Class
Bldg A3	1.04	-0.48	Very high	-0.3	Very high
Bldg A4	1.10	-0.55	Very high	-0.3	Very high

As presented in Table 2.7, the vulnerability class of two low-rise school buildings built in 1973 on soil class D and having concrete frames with infill masonry walls were calculated using the new VI equation to consider the influence of soil-building resonance effects. The results show that the very high vulnerability class before the introduction of the soil-building resonance parameter presents no difference, except an expectation of more building damage.

The results of the vulnerability assessment of another school campus composed of six mid-rise buildings (School 6 in Appendix I) built in 1968 on site class D and having concrete shear walls are shown in Table 2.8. All six buildings have a very high vulnerability class when the possible soil-building resonance effect is considered, compared to three with Tischer's method.

Table 2.8 Comparison of the vulnerability class according to the AHP-based method considering soil-building resonance and Tischer's adapted screening for a school campus of 6 buildings (School 6 in Appendix I)

Building	Coefficient of resonance	Analytical equation results (AHP)	Vulnerability Class	Adapted screening method	Vulnerability Class
1	1.02	0.10	Very high	2.3	Low
2	1.05	-0.46	Very high	-0.1	Very high
3	1.05	0.10	Very high	2.3	Low
4	1.02	-0.49	Very high	-0.1	Very high
5	1.02	-0.42	Very high	0.3	High
6	1.02	-0.49	Very high	-0.1	Very high

The increase of the vulnerability class from low to very high in some cases is related to the presence of soil-building resonance in the presence of soil type D or E. It can be noted that the very high vulnerability class does not necessarily mean a total building collapse as explained in Section 1.2.2.1. Furthermore, this increase of the structural vulnerability class does not affect the seismic risk of OFCs to the same extent, as will be explained in Chapter 3.

From these comparisons, it is seen that the consideration of soil-building resonance effects as included in the AHP-based method, strongly affect the vulnerability class of the buildings with natural frequency close to that of the underlying soil when the soil class is poor (Site Class D or E).

The calibration of the improved VI was conducted to ensure that the results from Tischer's adapted screening method and the AHP- based method give the same vulnerability classes for the buildings that are not prone to soil-building resonance.

2.6 Limitations

This chapter presented the development of a new seismic structural vulnerability equation in order to account for possible soil-building resonance effects. It is important to note that this remains an approximate method since the AHP scoring is based on engineering judgement and the assumption of statistical independence of the parameters. In this study, the new building vulnerability index is meant to be used for the seismic risk assessment of OFCs.

CHAPTER 3

NEW OFC SEISMIC RISK INDEX ACCORDING TO THE CSA S832 METHOD

In this chapter, the seismic risk index proposed in the parametric method of CSA-S832 is improved using the building vulnerability index calculated according to the AHP method presented in the previous chapter, and the revised method is applied to the OFCs inspected in the Montréal school buildings discussed in Chapter 2. The new seismic vulnerability index is classified from very low to high and the effects of the structural irregularities, year of construction and soil-building resonance, as well as local seismicity obtained from micro-zonation, are taken into consideration.

3.1 Setting building vulnerability index limits

It is proposed to improve the evaluation of the OFC seismic risk index of the CSA S832 method by introducing new structural parameters affecting the seismic risk of both the drift- and acceleration-sensitive components. The improvement essentially comes from a more refined evaluation of the seismic structural vulnerability index using AHP, while essentially keeping the existing OFC consequence rating (C) and individual component vulnerability index, V_E, as prescribed in CSA S832-14.

In order to keep the range of the OFC risk index, R, within the same limits as proposed in the CSA S832, calibration had to be done as described next. The lowest value of R was of no concern as the refined V values would not affect it, while calibration was necessary in the higher range to reflect the spectrum of Canada's uniform seismic hazard map. The highest value of R can be calculated by taking the highest V_G and V_B scores presented in CSA S832, for any consequence rating C. The maximum V_G is calculated for Tofino, British Colombia, which has the highest seismic hazard in Canada according to NBC with a design spectral acceleration of Sa (0.2) = 1.2 g. The highest value of V_G for a site class C is calculated according to Equation (3.1).

$$V_G = F_a S_a\,(0.2)/1.25 \tag{3.1}$$

For $F_a = 1$ and $S_a\,(0.2) = 1.2$, the maximum value of V_G is 0.96. In comparison, the value of the ground motion characteristic V_G used in Montréal for the studied buildings is 0.55, which is almost half of the value to be considered in Tofino. This means that if an identical building (and its OFCs) were located in Tofino with similar soil conditions, its seismic risk would nearly double. The limits of the OFC seismic risk according to CSA S832 are calculated by taking a worst-case study building using Equations (3.2) and (3.3).

$$R = V*C \tag{3.2}$$

$$V = V_G * V_B * V_E/10 \tag{3.3}$$

As indicated above, the maximum value of V_G is 0.96 and the maximum possible value of V_B is 1.5 according to CSA S832. Recall that V_E will be unchanged for the individual elements and its values were taken directly from the McGill study based on in situ OFC inspections. According to Table 1.10, the highest value of V_E is equal to 100 while the highest value of the consequences rating C according to Table 1.11 is equal to 20.

Replacing all these maximum values in Equations (3.2) and (3.3) yields a maximum OFC vulnerability score V of 14.4 and a maximum OFC seismic risk index R of 288.

3.2 Improvement of the OFC seismic risk index with effect of the variation of the local seismicity

For this study, V_G is equal to 0.55 representing Montréal seismicity and V_E depends on the vulnerability parameter of each OFC. In the proposed new procedure, V_B as used in CSA S832 will be replaced by V'_B taken as the inverse of the building seismic vulnerability index (VI)

resulting from AHP and including the effect of soil-building resonance parameter in replacement of the CSA S832-14 soil condition as parameter. V'_B is the inverse of VI because the vulnerability class is higher when VI is very low or negative. Moreover, the OFC seismic risk index R is directly proportional to V_B, which is the opposite to the case of VI. Therefore, in order to be consistent with the scale of the OFC seismic risk R defined in CSA S832, for any very high vulnerability class, VI will be taken as 0.2, which represents the maximum value of a very high vulnerability class. So, if the vulnerability class is very high then the maximum value of V'_B is 5, whereas the current limit of V_B is 1.5 in the CSA S832.

Therefore, the product of V'_B maximum (5) and V_G (0.55 for Montréal) will be equal to 2.75 for the case studies considered herein. But V'_B should be calibrated to not exceed the limit of 1.5, so it needs to be multiplied by 0.30 (1.5/5).

3.3 New OFC seismic risk index for a case study building in Montréal

The selected five-story case study building is prone to possible soil building resonance since its coefficient of resonance equals 1.04. Therefore, the OFCs located in this building are expected to be affected by this structural vulnerability parameter in addition to the presence of both plan and vertical irregularities. The characteristics of the studied building (School 16 in Appendix I) are represented in Table 3.1.

Table 3.1 Characteristics of the case study school building (School 16 in Appendix I).

Building	**LLRS**	**Year of Construction**	**Irregularities**		**Soil**	**Height of building**
			Plan	**Vertical**		
T	Concrete moment frames	1969	Yes	Yes	E	Mid rise

The effect of soil-building resonance on the seismic structural vulnerability of this building was already studied in Chapter 2 and the results are shown in Table 2.6. In this chapter, the same seismic structural vulnerability index from AHP will be used in the estimation of the seismic risk of the critical OFCs.

The seismic structural vulnerability VI of this case study building is negative according to Table 2.6, which corresponds to very high structural vulnerability class. Therefore, the vulnerability index will be taken as 0.2 and the V'_B is equal to (1/0.2) * 0.30 = 1.5 (the maximum possible value according to CSA S832).

3.3.1 Drift-sensitive components

The new seismic risk index is evaluated for drift-sensitive components such as the architectural components and for the acceleration-sensitive components such as the mechanical, electrical, and service components. These components can be strongly affected by a possible soil-building resonance as inter-story drifts will be increased by resonance. The drift-sensitive components of the case study building are presented in Table 3.2.

Table 3.2 Drift-sensitive components located in Building T

Name of OFC	Type	Localization
Classic suspended ceiling	INT	All floors
Glazing windows	INT	All floors
Staircase walls	INT	Gym
Raised passage	INT	Delivery entry
Concrete Staircase	INT	All floors Emergency exit
Unreinforced masonry walls (in plane response)	EXT	All floors
Stucco ceiling	INT	Auditorium
HVAC duct	MEC	All floors
Hot water piping	MEC	All floors
Fire pipes	MEC	All floors

The type INT in Table 3.2 represents internal components, the type EXT represents the external infill walls and the type MEC represents the mechanical components considered as drift sensitive.

The new seismic risk index of the critical drift-sensitive components listed in Table 3.2 is calculated for V'_B= 1.5 and V_G= 0.55. The results and the comparison with the results from a previous study using the CSA S832 parametric method are shown in Table 3.3.

Note that not all the drift-sensitive components are affected by the soil building resonance, neither by the structural irregularities so that their risk index will not be modified for them. For example, if the OFC is in the basement it will not be affected by any type of irregularities neither by the soil-building resonance.

Table 3.3 Comparison of the improved seismic risk index of the critical drift-sensitive components with the existing risk according to CSA S832

OFC type	**V_E**	**$V'_B * V_G * V_E/10$**	**C**	**New seismic R**	**Risk level**	**Seismic risk according to CSA**	**Risk level**
Classic suspended ceiling	55	4.54	15	68	High	54	Moderate
Glazing windows	48	3.96	15	59	Moderate	47	Moderate
Staircase walls	32	2.64	15	40	Moderate	31	Low
Raised passage	14	1.16	15	17	Low	14	Negligible
Concrete Staircase	12	1	15	15	Negligible	12	Negligible
Masonry walls	12	1	15	15	Negligible	12	Negligible
Stucco ceiling	12	1	15	15	Negligible	12	Negligible
HVAC duct	71	5.86	11	65	High	51.5	Moderate
Hot water piping	53	4.37	11	48	Moderate	38.5	Moderate
Fire pipes	26	2.15	20	43	Moderate	34.3	Moderate

The classification of the new seismic risk index according to the scale of CSA S832 is presented in Table 3.4.

Table 3.4 Suggested mitigation priority thresholds according to CSA S832

Risk Index	**Seismic Risk Level**	**Mitigation Priority**
R ≤16	Negligible	Not required
16 < R ≤ 32	Low	Low
32 < R ≤ 64	Moderate	Medium
64 < R ≤ 128	High	High
R > 128	Very high	Very high

As shown in Table 3.3, the new seismic risk index values have increased by 25% while the seismic risk level has only increased from medium to high for the suspended ceiling and from low to moderate for the staircase walls. This building had a $V_B = 1.2$ according to the current CSA S832 method and the 25% increase represents essentially the increase of V_B effects, from 1.2 to 1.5 due to the presence of the structural irregularities and the possible soil-building resonance in poor soil conditions.

3.3.2 Acceleration-sensitive components

In addition to the critical drift-sensitive components, the improved seismic risk index was also determined for the critical acceleration-sensitive components located in the case study building, listed in Table 3.5. The improved seismic risk index for these components considers the increased floor accelerations due soil-building resonance in addition to the other structural parameters.

During this study, the amplification of the acceleration is represented by the vulnerability of the component, V_E, since the CSA S832 parametric method has already taken into account the

location of the component in the building by determining the RS4 vulnerability parameter (see Table 1.10).

Table 3.5 Critical acceleration-sensitive components located in Building T

Name of OFC	Type	Localization
Heaters	E&IT	All floors
Ventilator	MEC	Roof top
Storage lockers	GEN	3rd floor

The type E&IT presented in Table 3.5 represents the electrical components, GEN represents the general components and the type MEC represents the mechanical components

Table 3.6 Comparison of the improved seismic risk index of the critical acceleration-sensitive components.

OFC type	V_E	$V'_B * V_G * V_E/10$	C	New seismic R	Risk level	Seismic risk according to CSA	Risk level
Heater	55	4.54	11	50	Moderate	40	Moderate
Storage lockers	12	1	11	11	Negligible	8.7	Negligible
Ventilator	46	3.8	20	76	High	61	Moderate

Table 3.6 presents the results of the evaluated new seismic risk of acceleration-sensitive components and the comparison with the previous results obtained with the CSA S832 method. It is seen that the seismic risk value has increased without affecting the risk level of heaters and lockers that remained the same as in the CSA results. The risk level of the ventilator has increased from moderate to high, mainly because of the increase of V_B due to the presence of

the irregularities and soil-building resonance. Note that many other acceleration-sensitive components are critical for post-earthquake functionality such as the emergency power generator, the electrical transformer and the water tank, but these components are located in the basement so they are not affected by the structural irregularities or by the possible soil-building resonance.

3.4 Effect of the seismicity on the OFC seismic risk

In order to illustrate the effect of the local seismicity on the results, all the above calculations were repeated for this same case study building but for different locations: Tofino ($V_G = 0.96$), Victoria ($V_G = 0.92$) where the population is higher than Tofino, St-Georges-de-Cacouna ($V_G = 0.78$ – the maximum in Québec), Québec City ($V_G = 0.48$) and Ottawa ($V_G = 0.55$) that is taken because of having similar seismicity to Montréal. Table 3.7 presents the results of the comparison.

Table 3.7 Improved seismic risk index, R, for drift-sensitive components with different seismicity

Name of OFC	**Tofino**	**Victoria**	**St-Georges-de-Cacouna**	**Montréal/Ottawa**	**Québec City**
Classic suspended ceiling	119	114	97	68	59
Glazing windows	104	99	84	59	52
Staircase walls	69	66	52	40	35
Raised passage	30	29	25	17	15
Concrete Staircase	26	25	21	15	13
Masonry walls (in plane)	26	25	21	15	13
Stucco ceiling	26	25	21	15	13
HVAC duct	113	108	91	65	56
Hot water piping	84	80	68	48	42
Fire pipes	75	72	61	43	37

Table 3.8 Seismic risk index, R, according to CSA S832 for drift-sensitive components with different seismicity

Name of OFC	**Tofino**	**Victoria**	**St-Georges-de-Cacouna**	**Montréal/Ottawa**	**Québec City**
Classic suspended ceiling	95	91	77	54	47
Glazing windows	83	80	67	47	41
Staircase walls	55	53	45	31	28
Raised passage	24	23	20	14	12
Concrete Staircase	21	20	17	12	10
Masonry walls (in plane)	21	20	17	12	10
Stucco ceiling	21	20	17	12	10
HVAC duct	90	86	73	51	45
Hot water piping	67	64	55	38	33
Fire pipes	60	57	49	34	30

The comparison between the results shown in Tables 3.7 and 3.8 indicates that the seismic risk index of drift sensitive OFCs increased by considering the soil-building resonance and building

irregularities. It is also seen that the higher seismicity will affect more the seismic risk of drift-sensitive OFCs with the possible occurrence of soil-building resonance. Moreover, the improved seismic risk is 25% larger than the current one for most of the studied OFCs according to CSA for the same seismicity. The difference in risk value between two cities represents the difference of V_G values. For example, the difference in risk value between Tofino City (V_G=0.96) and Montréal (V_G=0.55) is 75% which represents (0.96-0.55)/0.55. Moreover, the risk values of the classic suspended ceiling are equal to 119 for Tofino City and 68 for Montréal as shown in Table 3.7, the difference is (119-68)/68 which is also 75% higher.

Table 3.9 shows the effect of the seismicity on the improved seismic risk index for acceleration-sensitive components. The difference in risk value is the same as for the drift-sensitive components. The comparison between the results shown in Tables 3.9 and 3.10 indicates that the seismic risk of acceleration sensitive OFCs is affected by the soil-building resonance and the presence of structural irregularities.

Table 3.9 Improved seismic risk index, R, for acceleration-sensitive components with different seismicity

Name of OFC	**Tofino**	**Victoria**	**St-Georges-de-Cacouna**	**Montréal/Ottawa**	**Québec City**
Heater	87.1	84	71	50	44
Storage lockers	19.2	18	15	11	10
Ventilator	132	127	105	76	66

Table 3.10 Seismic risk index, R, according to CSA S832 for acceleration-sensitive components with different seismicity

Name of OFC	Tofino	Victoria	St-Georges-de-Cacouna	Montréal/Ottawa	Québec City
Heater	70	66.8	56.6	40	35
Storage lockers	15.2	14.6	12.4	8.7	7.6
Ventilator	106	101.6	86.1	61	53

3.5 Observations

Results indicate that the integration of new structural parameters in the building vulnerability index, has increased the level of risk for some OFCs. The comparison between the results can be considered as straight forward, since the scale of risk level according to CSA S832 was respected, which is especially important in the upper limits. Moreover, the influence of the seismicity on the OFC seismic risk was also analyzed using the V_G values of five different locations in Canada (West and East), and the results show how the seismicity strongly affects the seismic risk of OFCs. For example, the risk level of the classic suspended ceiling is moderate according to the CSA in a moderate seismicity (Montréal/Ottawa) and this level has increased to be very high as shown in Table 3.8. In addition, the risk level of the suspended ceiling is getting higher with the highest seismicity (Tofino) and close to be very high seismic risk after the integration of the new parameters.

CHAPTER 4

SUMMARY AND CONCLUSIONS

The main objective of this study was to propose an improved seismic risk index associated to the operational and functional (non-structural) components (OFCs) located in some secondary schools designated as post-disaster shelters in Montréal. Sixteen schools comprising 101 buildings are designated as post-disaster shelters by the civil safety department of the City of Montréal. The characteristics of the school buildings and their OFCs were taken from a previous study conducted at McGill University. The available data allowed fulfilling a specific objective of the research, which was to introduce the effect of soil-building resonance on the seismic structural and non-structural vulnerabilities of the school buildings.

4.1 New seismic structural vulnerability index

The structural vulnerability index, VI, was computed according to the Analytical Hierarchy Process AHP method. It is a score assignment method based on the adapted seismic screening method by FEMA 154. The final value of the seismic structural vulnerability index is calculated as the sum of the structural parameters multiplied by the weight factor of each. The parameters considered are the lateral load resisting system (LLRS), building height, year of construction, presence of structural irregularities (in-plane and vertical) and the soil-building resonance, the latter as a new parameter contributing to the structural vulnerability. The improved structural vulnerability index was used to compute the seismic risk of operational and functional components (OFCs) with consideration of the effect of soil-building resonance, i.e. increased floor accelerations and inter-story drift values. The soil-building resonance was represented by a coefficient equal to the ratio of the fundamental frequency of the local soil and the fundamental frequency of the school building ($f_{soil}/f_{structure}$).

The results obtained with the new parameters were validated and found to comply with those obtained from the adapted screening method developed by Tischer (Tischer, 2012) in 97% of the cases considered. Moreover, the study showed that possible soil-building resonance effects are an important factor when the soil conditions are poor (actually the highest contribution according to the AHP approach) and it should be considered in the building vulnerability assessment.

4.2 New OFC seismic risk index

The new OFC seismic risk index is an index based on the CSA S832 standard (Seismic risk reduction of operational and functional components of buildings), with improved considerations in the assessment of the building vulnerability to include the relative importance of other parameters such as year of construction, presence of structural irregularities as well as soil-building resonance, currently not accounted for in the CSA S832 parametric method.
The new building vulnerability index was calibrated such that the upper limits of the current OFC seismic risk index, R, according to CSA were kept unchanged and the same scale of risk level could be used.

The results of the study showed that the introduction of the new structural vulnerability parameters refines the vulnerability assessment of the buildings and provides compatibility with the framework of the FEMA score procedure as previously enhanced by Tischer (Tischer, 2012).

4.3 Conclusions

The present research involved the improvement of the rapid seismic structural vulnerability assessment method developed by Tischer (2012) by introducing a new ranking approach for parameters affecting the vulnerability. The proposed methodology using the AHP has identified the percentage of contribution for each parameter considered in the assessment of the seismic structural vulnerability of school buildings designated as post-disaster shelters in

Montréal. Based on the analysis, it was identified that the effects of soil-building resonance and structural irregularities have the highest contribution in the seismic structural vulnerability. As part of this research project, ambient vibration measurements were taken at specified local sites to estimate the reliability of its use while calculating the coefficient of soil-building resonance. Furthermore, the obtained seismic risk index obtained for the building structures were compared with those from Tischer's study and showed a large difference between the results, especially for the buildings prone to soil-building resonance in poor soil sites.

The determination of an improved OFC seismic risk index was conducted by taking into account new structural parameters that were not considered in the CSA S832 such as the structural irregularities, the year of construction and the effect of soil-building resonance. Moreover, the effect of soil-building resonance on the seismic risk of OFCs was identified in detail with the variation of the local seismicity and the obtained results confirm that this effect increases if the building is located in higher seismicity.

The goal of the present study was to the improve the seismic structural vulnerability score that is used to assess the seismic risk of OFCs and therefore has the limitations related to the AHP methodology. The proposed improvement does not include a detailed assessment and is based on rapid screening evaluation method. Moreover, the limitations exist regarding the comparison between the rapid visual screening method and the AHP based method due to the assumption of the weight factors via pairwise comparison. In addition, the improved seismic risk index is limited with the scale of risk mitigation according to CSA S832. Furthermore, this method still does not provide the real relation between the seismic risk of OFCs and the structural vulnerability since it is based on limited visual inspection scores. Also, the effect of soil-building resonance on the seismic risk of OFCs is also limited by the term V'_B.

A more detailed assessment is still required to confirm the actual vulnerability of the highly vulnerable buildings to confirm the need for mitigation. Moreover, a deeper investigation could be done with detailed modeling and dynamic analysis for some vulnerable buildings.

4.4 Suggestions for future work

Based on the conclusions and limitations of this study, some suggestions for future work are as follows:

- The soil condition and the soil-building resonance need more detailed investigation as effects of resonance with weaker soils may be more important for drift than for accelerations. Comparative studies could be done by modeling a building with a flexible base that represents the soil parameters in order to ascertain whether the soil condition need to be considered as a parameter when considering the possible resonance in the assessment of the structural vulnerability.
- The seismic risk index is still calculated for individual OFC types; therefore, there is a need for a method that can represent a global risk index of OFCs located in one building.
- A relation between the seismic vulnerability of individual OFCs and subsystems and the structural vulnerability can be explored using a reliability-based approach to determine the feasibility of using one post-earthquake functionality index representing the global vulnerability index (building and its OFCs).
- A nonlinear seismic analysis study of some of the buildings considered as shelters could be conducted in order to get their OFC fragility curves and validate whether the rapid screening method gives comparable risk levels.
- A detailed assessment of the effect of soil-building resonance on the amplification of the floor acceleration and displacement that can affect the response of OFCs.

APPENDIX I

CHARACTERISTICS OF SCHOOL BUILDINGS IN MONTRÉAL

Table-A I-1 Characteristics of School 1

Building	LLRS	Year of Construction	Irregularities		Soil	Building height
			Plan	Vertical		
A1	Concrete frames with infill masonry shear walls	1973	Yes	No	D	Mid rise
A2	Concrete frames with infill masonry shear walls	1973	Yes	No	D	Mid rise
A3	Concrete frames with infill masonry shear walls	1973	Yes	Yes	D	Mid rise
A4	Concrete frames with infill masonry shear walls	1973	Yes	Yes	D	Mid rise
B1	Concrete frames with infill masonry shear walls	1973	yes	yes	D	Mid rise
B2	Concrete frames with infill masonry shear walls	1973	Yes	Yes	D	Mid rise
B3	Concrete frames with infill masonry shear walls	1973	No	No	D	Low rise
C1	Concrete frames with infill masonry shear walls	1973	No	No	D	Low rise
C2	Steel moment frame	1973	Yes	Yes	D	Low rise
C3	Steel moment frame	1973	Yes	Yes	D	Low rise

Table-A I-2 Characteristics of School 2

Building	LLRS	Year of Construction	Irregularities		Soil	Building height
			Plan	Vertical		
A1	Concrete frames with infill masonry shear walls	1964	yes	yes	E	Low rise
A2	Precast concrete frame	1964	No	Now	E	Low rise
B1	Precast concrete frame	1964	No	No	E	Low rise
B2	Concrete frames with infill masonry shear walls	1964	No	Yes	E	Low rise
C	Concrete frames with infill masonry shear walls	1964	yes	No	E	Low rise
3	Steel moment frame	1970	No	Yes	E	Low rise
4	Steel moment frame	1970	No	Yes	E	Low rise

Table-A I-3 Characteristics of School 3

Building	LLRS	Year of Construction	Irregularities		Soil	Building height
			Plan	Vertical		
1A	Concrete frames with infill masonry shear walls	1962	yes	yes	C	Low rise
1B	Concrete frames with infill masonry shear walls	1962	No	yes	C	Low rise
1C	Concrete frames with infill masonry shear walls	1962	No	Yes	C	Low rise
2A	Steel moment frame	1973	No	Yes	C	Low rise
2B	Steel moment frame	1973	yes	yes	C	Low rise
3	Steel moment frame	1973	No	Yes	C	Low rise
4A	Steel moment frame	1973	No	Yes	C	Low rise
4B	Steel moment frame	1973	No	Yes	C	Low rise
5A	Steel frame with infill masonry shear walls	1973	No	Yes	C	Low rise
5B	Steel frame with infill masonry shear walls	1973	No	Yes	C	Low rise

Table-A I-4 Characteristics of School 4

Building	LLRS	Year of Construction	Irregularities		Soil	Building height
			Plan	Vertical		
A	Precast concrete frame	1972	yes	yes	E	Low rise

Table-A I-5 Characteristics of School 5

Building	LLRS	Year of Construction	Irregularities		Soil	Building height
			Plan	Vertical		
A1	Concrete frames with infill masonry shear walls	1967	yes	yes	C	Low rise
A2	Concrete frames with infill masonry shear walls	1967	No	yes	C	Low rise
A3	Concrete frames with infill masonry shear walls	1967	Yes	Yes	C	Low rise
B1	Concrete frames with infill masonry shear walls	1967	No	No	C	Low rise
B2	Concrete shear walls	1967	No	yes	C	Low rise
B3	Concrete frames with infill masonry shear walls	1967	No	Yes	C	Low rise
C1	Concrete frames with infill masonry shear walls	1967	Yes	Yes	C	Low rise
C2	Concrete frames with infill masonry shear walls	1967	Yes	Yes	C	Low rise
C3	Concrete frames with infill masonry shear walls	1967	Yes	Yes	C	Low rise

Table-A I-6 Characteristics of School 6

Building	LLRS	Year of Construction	Irregularities		Soil	Building height
			Plan	Vertical		
1	Concrete shear walls	1968	No	yes	D	Mid rise
2	Concrete frames with infill masonry shear walls	1968	Yes	yes	D	Mid rise
3	Concrete shear walls	1968	No	Yes	D	Mid rise
4	Concrete shear walls	1968	Yes	Yes	D	Low rise
5	Concrete shear walls	1968	yes	yes	D	Mid rise
6	Concrete shear walls	1968	Yes	Yes	D	Low rise

Table-A I-7 Characteristics of School 7

Building	LLRS	Year of Construction	Irregularities		Soil	Building height
			Plan	Vertical		
1	Steel frame with infill masonry shear walls	1956	Yes	No	C	Low rise
2	Concrete frames with infill masonry shear walls	1983	No	yes	C	Low rise

Table-A I-8 Characteristics of School 8

Building	LLRS	Year of Construction	Irregularities		Soil	Building height
			Plan	Vertical		
A	Steel moment frame	1963	yes	yes	C	Low rise
B	Steel frame with infill masonry shear walls	1963	No	yes	C	Low rise
B’	Steel frame with infill masonry shear walls	1968	Yes	No	C	Low rise
C	Concrete moment frame	1963	No	No	C	Low rise
D	Steel frame with infill masonry shear walls	1970	No	No	C	Low rise
E	Concrete frames with infill masonry shear walls	1970	Yes	No	C	Low rise
F	Concrete shear walls	1970	No	No	C	Low rise

Table-A I-9 Characteristics of School 9

Building	LLRS	Year of Construction	Irregularities		Soil	Building height
			Plan	Vertical		
A	Concrete frames with infill masonry shear walls	1987	yes	No	C	Low rise
B	Concrete frames with infill masonry shear walls	1987	Yes	yes	C	Low rise
C	Steel moment frame	1987	Yes	No	C	Low rise
D	Concrete frames with infill masonry shear walls	1987	Yes	No	C	Low rise
E	Steel moment frame	1988	yes	No	C	Low rise
P	Steel braced frame	1989	Yes	No	C	Low rise

Table-A I-10 Characteristic of School 10

Building	LLRS	Year of Construction	Irregularities		Soil	Building height
			Plan	Vertical		
A	Concrete shear walls	1970	yes	yes	E	Mid rise
B	Concrete moment frame	1970	No	No	E	Mid rise
C	Concrete shear walls	1970	Yes	Yes	E	Mid rise
D	Concrete shear walls	1970	Yes	Yes	E	Low rise

Table-A I-11 Characteristics of School 11

Building	LLRS	Year of Construction	Irregularities		Soil	Building height
			Plan	Vertical		
A	Steel moment frame	1982	yes	yes	C	Low rise
C	Concrete frames with infill masonry shear walls	1982	No	yes	C	Low rise
S	Concrete frames with infill masonry shear walls	1982	No	No	C	Low rise
E	Concrete frames with infill masonry shear walls	1982	No	No	C	Low rise

Table-A I-12 Characteristics of School 12

Building	LLRS	Year of Construction	Irregularities		Soil	Building height
			Plan	Vertical		
A	Concrete frames with infill masonry shear walls	1971	yes	No	C	Low rise
B	Concrete shear walls	1971	No	yes	C	Low rise
C	Concrete frames with infill masonry shear walls	1971	No	Yes	C	Low rise
D	Concrete shear walls	1971	No	No	C	Low rise
E	Concrete frames with infill masonry shear walls	1971	No	No	C	Low rise
F	Steel frame with infill masonry shear walls	2001	No	No	C	Low rise

Table-A I-13 Characteristics of school 13

Building	LLRS	Year of Construction	Irregularities		Soil	Building height
			Plan	Vertical		
A	Concrete frames with infill masonry shear walls	1964	No	Yes	A	Low rise
B	Concrete frames with infill masonry shear walls	1964	Yes	Yes	A	Low rise
B’	Concrete frames with infill masonry shear walls	1964	Yes	No	A	Low rise
C	Concrete shear walls	1973	No	Yes	A	Low rise
C’	Concrete shear walls	1973	yes	No	A	Low rise

Table-A I-14 Characteristics of School 14

Building	LLRS	Year of Construction	Irregularities		Soil	Building height
			Plan	Vertical		
A	Steel moment frame	1968	No	No	E	Low rise
B1	Concrete moment frame	1968	Yes	Yes	E	Low rise
B2	Concrete moment frame	1968	No	Yes	E	Low rise
B3	Concrete moment frame	1968	Yes	Yes	E	Low rise
C1	Concrete frames with infill masonry shear walls	1968	Yes	No	E	Low rise
C2	Concrete frames with infill masonry shear walls	1968	Yes	No	E	Low rise
D	Concrete moment frame	1968	No	No	E	Low rise
E	Concrete moment frame	1968	Yes	Yes	E	Low rise

Table-A I-15 Characteristics of School 15

Building	LLRS	Year of Construction	Irregularities		Soil	Building height
			Plan	Vertical		
A	Concrete shear walls	1972	No	No	B	Low rise
B	Concrete shear walls	1972	Yes	Yes	B	Low rise
C	Steel moment frame	1972	No	No	B	Low rise
D	Concrete shear walls	1972	Yes	No	B	Low rise

Table-A I-16 Characteristics of School 16

Building	LLRS	Year of Construction	Irregularities		Soil	Height of building
			Plan	Vertical		
T	CMF	1969	yes	yes	E	Mid rise
U	CMF	1969	No	yes	E	Mid rise
V	CSW	1969	No	No	E	Mid rise
W	CSW	1969	No	No	E	Mid rise
X	CSW	1969	yes	yes	E	Mid rise
Y	CSW	1969	No	No	E	Low rise
Z	CSW	1969	No	No	E	Low rise
S	CSW	1974	yes	No	E	Low rise

APPENDIX II

DYNAMIC PROPERTIES OF THE STUDIED BUILDINGS AND THE ADJACENT SOIL

The following tables present the fundamental frequencies of the school buildings and the adjacent soil obtained from AVM.

Table-A II-1 Fundamental frequencies for soil and buildings of School 1

Building	Soil Frequency (Hz)	Building frequency (Hz)
A1	10.31	4.9
A2	10.31	4.86
A3	10.31	10.05
A4	10.31	9.4
B1	10.31	4.86
B2	10.31	3.87

Table-A II-2 Fundamental frequencies for soil and buildings of School 2

Building	Soil Frequency (Hz)	Building frequency (Hz)
A1	17.56	4.76
A2	17.56	4.78
B1	17.56	4.24
B2	17.56	9.09
C	17.56	4.17
3	17.56	7.96
4	17.56	5.32

Table-A II-3 Fundamental frequencies for soil and buildings of School 3

Building	Soil Frequency (Hz)	Building frequency (Hz)
1A	14.38	5.00
1B	14.38	5.56
1C	14.38	5.56

Table-A II-4 Fundamental frequencies for soil and buildings of School 4

Building	Soil Frequency (Hz)	Building frequency (Hz)
A	16.72	3.53

Table-A II-5 Fundamental frequencies for soil and buildings of School 5

Building	Soil Frequency (Hz)	Building frequency (Hz)
A1	51.56	4.55
A2	51.56	4.55
A3	51.56	4.55
B1	51.56	4.55
B2	51.56	4.55
B3	51.56	4.55
C1	51.56	4.55
C2	51.56	4.55
C3	51.56	4.55

Table-A II-6 Fundamental frequencies for soil and buildings of School 6

Building	Soil Frequency (Hz)	Building frequency (Hz)
1	3.09	3.03
2	3.09	2.94
3	3.09	2.94
4	3.09	3.03
5	3.09	3.03
6	3.09	3.03

Table-A II-7 Fundamental frequencies for soil and buildings of School 7

Building	Soil Frequency (Hz)	Building frequency (Hz)
1	16.88	4.92
2	16.88	4.92

Table-A II-8 Fundamental frequencies for soil and buildings of School 8

Building	Soil Frequency (Hz)	Building frequency (Hz)
B	29.3	4.68
E	29.3	5.61

Table-A II-9 Fundamental frequencies for soil and buildings of School 9

Building	Soil Frequency (Hz)	Building frequency (Hz)
A	14.48	3.85
C	14.48	3.85
D	14.48	7.14

Table-A II-10 Fundamental frequencies for soil and buildings of School 11

Building	Soil Frequency (Hz)	Building frequency (Hz)
A	42.78	8.33
B	42.78	6.25
C	42.78	5.88
D	42.78	8.33
E	42.78	7.69

Table-A II-11 Fundamental frequencies for soil and buildings of School 12

Building	Soil Frequency (Hz)	Building frequency (Hz)
A	5.31	3.90
B	5.31	3.75
B'	5.31	3.90
C	5.31	3.75
C'	5.31	5.07

Table-A II-12 Fundamental frequencies for soil and buildings of School 14

Building	Soil Frequency (Hz)	Building frequency (Hz)
A	1.88	4.00
B	1.88	3.33
C'	1.88	1.77
D	1.88	1.77

APPENDIX III

VALIDATION OF THE AHP RESULTS WITH THE ADAPTED SEISMIC SCREENING METHOD

The following tables highlight results of the vulnerability class according to the AHP-based method and Tischer's method.

Table-A III-1 Comparison of structural vulnerability index and class according to the AHP-based method and Tischer's (2012) adapted screening method without the coefficient of resonance of School 1

Building	Analytical equation results (AHP)	Vulnerability class	Adapted screening method	Vulnerability class
A1	0.69	Moderate	1.7	Moderate
A2	0.69	Moderate	1.7	Moderate
A3	0.15	Very high	-0.3	Very high
A4	0.15	Very high	-0.3	Very high
B1	0.18	Very high	-0.1	Very high
B2	0.18	Very high	-0.1	Very high
B3	0.82	Low	2.2	Low
C1	0.82	Low	2.2	Low
C2	0.55	Moderate	1.5	Moderate
C3	0.55	Moderate	1.5	Moderate

Table-A III-2 Comparison of structural vulnerability index and class according to the AHP-based method and Tischer's (2012) adapted screening method without the coefficient of resonance of School 2

Building	Analytical equation results (AHP)	Vulnerability Class	Adapted screening method	Vulnerability Class
A1	0.04	Very high	-0.9	Very high
A2	0.58	Moderate	1.6	Moderate
B1	0.58	Moderate	1.6	Moderate
B2	0.15	Very high	-0.4	Very high
C	0.47	Moderate	1.1	Moderate
3	0.39	Moderate	1.4	Moderate
4	0.39	Moderate	1.4	Moderate

Table-A III-3 Comparison of structural vulnerability index and class according to the AHP-based method and Tischer's (2012) adapted screening method without the coefficient of resonance of School 3

Building	Analytical equation results (AHP)	Vulnerability Class	Adapted screening method	Vulnerability Class
1A	0.22	High	0.1	High
1B	0.35	High	0.6	High
1C	0.35	High	0.6	High
2A	0.79	Low	2.4	Low
2B	0.52	Moderate	1.9	Moderate
3	0.79	Low	2.4	Low
4A	0.79	Low	2.4	Low
4B	0.79	Low	2.4	Low
5A	0.44	High	0.8	High
5B	0.44	High	0.8	High
6	0.80	Low	2.2	Low

Table-A III-4 Comparison of structural vulnerability index and class according to the AHP-based method and Tischer's (2012) adapted screening method without the coefficient of resonance of School 4

Building	Analytical equation results (AHP)	Vulnerability Class	Adapted screening method	Vulnerability Class
A	0.17	Very high	-0.4	Very high

Table-A III-5 Comparison of structural vulnerability index and class according to the AHP-based method and Tischer's (2012) adapted screening method without the coefficient of resonance of School 5

Building	Analytical equation results (AHP)	Vulnerability Class	Adapted screening method	Vulnerability Class
A1	0.22	High	0.1	High
A2	0.35	High	0.6	High
A3	0.22	High	0.1	High
B1	0.35	High	0.6	High
B2	0.35	High	0.6	High
B3	0.35	High	0.6	High
C1	0.22	High	0.1	High
C2	0.22	High	0.1	High
C3	0.22	High	0.1	High
D	0.22	High	0.1	High

Table-A III-6 Comparison of structural vulnerability index and class according to the AHP-based method and Tischer's (2012) adapted screening method without the coefficient of resonance of School 6

Building	Analytical equation results (AHP)	Vulnerability Class	Adapted screening method	Vulnerability Class
1	0.83	Low	2.3	Low
2	0.18	Very high	-0.1	Very high
3	0.83	Low	2.3	Low
4	0.24	High	-0.1	Very high
5	0.29	High	0.3	High
6	0.24	High	-0.6	Very high

Table-A III-7 Comparison of structural vulnerability index and class according to the AHP-based method and Tischer's (2012) adapted screening method without the coefficient of resonance of School 7

Building	Analytical equation results (AHP)	Vulnerability Class	Adapted screening method	Vulnerability Class
1	0.84	Low	2.3	Low
2	0.35	High	0.6	High

Table-A III-8 Comparison of structural vulnerability index and class according to the AHP-based method and Tischer's (2012) adapted screening method without the coefficient of resonance of School 8

Building	Analytical equation results (AHP)	Vulnerability Class	Adapted screening method	Vulnerability Class
A	0.45	High	0.5	High
B	0.44	High	0.8	High
B'	0.84	Low	2.3	Low
C	0.83	Low	2.4	Low
D	0.98	Low	2.8	Low
E	0.75	Low	2.1	Low
F	1.19	Low	4.4	Low

Table-A III-9 Comparison of structural vulnerability index and class according to the AHP-based method and Tischer's (2012) adapted screening method without the coefficient of resonance of School 9

Building	Analytical equation results (AHP)	Vulnerability Class	Adapted screening method	Vulnerability Class
A	0.18	Very high	-0.1	Very high
B	0.53	Moderate	1.6	Moderate
C	0.18	Very high	-0.1	Very high
D	0.14	Very high	-0.5	Very high

Table-A III-10 Comparison of structural vulnerability index and class according to the AHP-based method and Tischer's (2012) adapted screening method without the coefficient of resonance of School 10

Building	Analytical equation results (AHP)	Vulnerability Class	Adapted screening method	Vulnerability Class
A	0.62	Moderate	1.9	Moderate
C	0.22	High	0.1	High
S	0.35	High	0.6	High
E	0.89	Low	2.6	Low

Table-A III-11 Comparison of structural vulnerability index and class according to the AHP-based method and Tischer's (2012) adapted screening method without the coefficient of resonance of School 11

Building	Analytical equation results (AHP)	Vulnerability Class	Adapted screening method	Vulnerability Class
A	0.75	Low	2.1	Low
B	1.05	Low	3.9	Low
C	0.75	Low	2.1	Low
D	1.06	Low	4.4	Low
E	0.35	High	0.6	High
F	0.98	Low	2.8	Low

Table-A III-12 Comparison of structural vulnerability index and class according to the AHP-based method and Tischer's (2012) adapted screening method without the coefficient of resonance of School 12

Building	Analytical equation results (AHP)	Vulnerability Class	Adapted screening method	Vulnerability Class
A	0.35	High	0.6	High
B	0.22	High	0.1	High
B'	0.75	Low	2.1	Low
C	1.05	Low	3.9	Low
C'	1.05	Low	3.9	Low

Table-A III-13 Comparison of structural vulnerability index and class according to the AHP-based method and Tischer's (2012) adapted screening method without the coefficient of resonance of School 13

Building	Analytical equation results (AHP)	Vulnerability Class	Adapted screening method	Vulnerability Class
A	0.82	Low	2	Low
B1	-0.01	Very high	-1.1	Very high
B2	0.1	Very high	-0.6	Very high
B3	-0.01	Very high	-1.1	Very high
C1	0.47	Moderate	1.1	Moderate
C2	0.47	Moderate	1.1	Moderate
D	0.53	Moderate	1.4	Moderate
E	-0.01	Very high	-1.1	Very high

Table-A III-14 Comparison of structural vulnerability index and class according to the AHP-based method and Tischer's (2012) adapted screening method without the coefficient of resonance of School 14

Building	Analytical equation results (AHP)	Vulnerability Class	Adapted screening method	Vulnerability Class
A	0.42	Moderate	1.6	Moderate
B	0.31	Moderate	1.1	Moderate
C	0.82	Low	3.4	Low
D	0.81	Low	3.1	Low

APPENDIX IV

DETAILED APPLICATION OF THE AHP-BASED METHOD AND THE ADAPTED SCREENING METHOD

A detailed example of calculation is given for Building T of the School 16 in APPENDIX I, is given as follows:

App. IV. 1. The detailed calculation of the VI using the adapted screening method

Table IV-I BSH and score modifiers of building T

Building	**LLRS (BSH)**	**Year of Construction**	**Irregularities**		**Soil**	**Height of building**
			Plan	**Vertical**		
T	CMF	1969	yes	yes	E	Mid rise
Scores	3.6	0	-2	-0.5	-1.6	0.4

BSH = 3 (Tables 1.3 and 1.4)

∑Score modifier = 0+(-2) + (-0.5) + (-1.6) + 0.4= -3.7 (Tables 1.3 and 1.4)

S= 3 + (0 – 2 – 0.5 – 1.6 + 0.4) = - 0.7 (very high vulnerability class according to Table 1.5)

App. IV. 2. The detailed calculation of the VI using the AHP based method

Equation (2.2) is used to calculate the VI and he detailed calculation for the same building characteristics and scores shown in Table I.1 is given as follow:

$$VI = a * b * c * d * \sum \boldsymbol{X_i} * P_i \qquad (2.2)$$

A, b and c are equal to 1 because the LLRS is CMF and E is equal to 0.8 because the soil is type E.

VI= 0.8 * (0.31*3+0.13*0 – 2.5*0.27 – 1.6*0.16 + 0.13*0.4) = 0.08 (Very high vulnerability class according to Table 2.3). This vulnerability class is without the effect of soil building resonance. The calculation of VI with the effect of soil building resonance is as follows:

VI= 0.8 * (0.23*3+0.12*0 – 2.5*0.2 – 1.6*0.31+ 0.13*0.4) = - 0.06 (Very high vulnerability class according to Table 2.3).

LIST OF BIBLIOGRAPHICAL REFERENCES

A/S. (2010). Structural Vibration Solutions ARTeMIS Extractor Handy (Version 5.0) [Software].

ATC. (1996). ATC-40 Seismic evaluation and retrofit of concrete buildings." Applied Technology Council, Redwood, CA.

ATC. (2002). FEMA154 Rapid visual screening of buildings for potential seismic hazard: A handbook. Applied Technology Council, Redwood, CA.

ATC. (2005). Improvement of nonlinear static seismic analysis procedures. *FEMA 440, prepared by Applied Technology Council (ATC-55 Project)*.

Bertogg, M., Hitz, L., & Schmid, E. (2002). *Vulnerability functions derived from loss data for insurance risk modelling: findings from recent earthquakes.* Proceedings of the twelfth European conference on earthquake engineering (paper 281), London.

Bolander, J. E., Hutchinson, T. C., & Berton, S. (2001). Dynamic Behavior of Simple Soil-Structure Systems, Student's Guide, Department of Civil and Enviromental Engineering, University of California at Davis, 2001.

Calvi, G. M., Pinho, R., Magenes, G., Bommer, J. J., Restrepo-Vélez, L. F., & Crowley, H. (2006). Development of seismic vulnerability assessment methodologies over the past 30 years. *ISET Journal of Earthquake Technology, 43*(3), 75-104.

Chakos, A. (2004). Learning about seismic safety of schools from community experience in Berkeley, California. *School Safety and Security. Keeping Schools Safe in Earthquakes*, 45-51.

Chouinard, L., & Rosset, P. (2011). *Microzonation of Montreal, variability in soil classification.* Proceeding of the 4th IASPEI/IAEE International Symposium, University of California SB.

CSA. (2014). Seismic Risk Reduction of Operational and Functional Components (OFCs) of Buildings, CAN/CSA/S832-14 CSA, Rexdale, Ontario.

D'Ayala, D., & Kansal, A. (2004). *Analysis of the seismic Vulnerability of the architectural Heritage in Buhj, Gujarat, India.* Structural Analysis of Historical Construction conference, pp 1069 -1078, 2004.

D'ayala, Meslem, A., Vamvastikos, D., Porter, K., Rossetto, T., Crowley, H., & Silva, V. (2014). Guidelines for analytical vulnerability assessment of low/mid-rise Buildings—Methodology. Vulnerability Global Component project. In: DOI: 10.13117/GEM.VULN—MOD.TR2014.12.

D'Ayala, & Paganoni, S. (2011). Assessment and analysis of damage in L'Aquila historic city centre after 6th April 2009. *Bulletin of Earthquake Engineering, 9*(1), 81-104.

D'Ayala, & Speranza, E. (2003). Definition of collapse mechanisms and seismic vulnerability of historic masonry buildings. *Earthquake Spectra, 19*(3), 479-509.

D'Ayala, D. (2004). *Correlation of fragility curves for vernacular building types: Houses in Lalitpur, Nepal and in Istanbul, Turkey.* Proceedings of the 13th World Conference of Earthquake Engineering, University of Bath, 2004.

Decanini, L., Di Pasquale, G., Galli, P., Mollaioli, F., & Sano, T. (2004). Seismic hazard and seismic zonation of the region affected by the 2002 Molise, Italy, earthquake. *Earthquake Spectra, 20*(1_suppl), 131-165.

Dolce, M. (2004). *Seismic safety of schools in Italy.* Keeping schools safe in earthquakes, ad hoc experts' group meeting on earthquake safety in schools, , Paris, February 9-11, 52-63.

FEMA454. (2006). Designing for Earthquakes: A Manual for Architects, Federal Emergency Management Agency. U.S

FEMA, F. (1997). NEHRP guidelines for the seismic rehabilitation of buildings. In: Federal Emergency Management Agency Washnigton, DC.

Freeman, S. A. (1998). *The capacity spectrum method.* Proceedings of the 11th European conference on earthquake engineering, 6-11 September, Paris, 1998.

Gehl, P., Douglas, J., Rossetto, T., Macabuag, J., Nassirpour, A., Minas, S., & Duffour, P. (2014). Investigating the use of record-to-record variability in static capacity approaches. In *Vulnerability, Uncertainty, and Risk: Quantification, Mitigation, and Management, pp. 1675-1684.*

Ghosh, S. K., & Cleland, N. (2012). Observations from the February 27, 2010, earthquake in Chile. *PCI journal, 57*(1).

HAZUS-MH, N. (2004). Users's manual and technical manuals. report prepared for the federal emergency management agency. *National Institute of Building Sciences*. Federal Emergency Management Agency (FEMA). Washington, DC.

HAZUS, N. (1999). Earthquake loss estimation technology. *Technical manual prepared by the National Institute of Buildings Sciences (NIBS) for the Federal Emergency Management Agency (FEMA)*.

Jalayer, F., & Cornell, C. (2009). Alternative non-linear demand estimation methods for probability-based seismic assessments. *Earthquake Engineering & Structural Dynamics*. *38*(8), 951-972.

Kelson, K. I., Kang, K.-H., Page, W. D., Lee, C.-T., & Cluff, L. S. (2001). Representative styles of deformation along the Chelungpu fault from the 1999 Chi-Chi (Taiwan) earthquake: geomorphic characteristics and responses of man-made structures. *Bulletin of the Seismological Society of America, 91*(5), 930-952.

Kircher, C. A., Nassar, A. A., Kustu, O., & Holmes, W. T. (1997). Development of building damage functions for earthquake loss estimation. *Earthquake Spectra, 13*(4), 663-682.

Kircher, C. A., Whitman, R. V., & Holmes, W. T. (2006). HAZUS earthquake loss estimation methods. *Natural Hazards Review, 7*(2), 45-59.

Kvasnicka, P., Matesic, L., & Ivandic, K. (2011). Geotechnical site classification and Croatian National Annex for Eurocode 8/Geotehnicka klasifikacija tla i hrvatski Nacionalni dodatak Eurokodu 8. *Geofizika, 28*(1), 83-98.

Lin, P., & Wang, N. (2017a). Stochastic post-disaster functionality recovery of community building portfolios I: Modeling. *Structural Safety, 69*, 96-105.

Lin, P., & Wang, N. (2017b). Stochastic post-disaster functionality recovery of community building portfolios II: Application. *Structural Safety, 69*, 106-117.

López, O. A., Hernández, J. J., Del Re, G., Puig, J., & Espinosa, L. (2007). Reducing seismic risk of school buildings in Venezuela. *Earthquake Spectra, 23*(4), 771-790.

McAdoo, B. G., Dengler, L., Prasetya, G., & Titov, V. (2006). How an oral history saved thousands on Indonesia's Simeulue Island during the December 2004 and March 2005 tsunamis. *Earthquake Spectra, 22*(3_suppl), 661-669.

McConnell, V. (2007). Statewide seismic needs assessment: Implementation of Oregon 2005 Senate Bill 2 relating to public safety, earthquakes, and seismic rehabilitation of public buildings. *State of Oregon, Department of Geology and Mineral Industries, Portland, OR*. doi:http://www.oregongeology.org/sub/projects/rvs/default.htm.

Micromed, S. (2011). Software Grilla. http://www.tromino.it/frameset-grilla.htm.

Mucciarelli, M., Masi, A., Gallipoli, M. R., Harabaglia, P., Vona, M., Ponzo, F., & Dolce, M. (2004). Analysis of RC building dynamic response and soil-building resonance based on data recorded during a damaging earthquake (Molise, Italy, 2002). *Bulletin of the Seismological Society of America, 94*(5), 1943-1953.

Nakamura, Y. (2010). Yutaka Nakamura; Comment on "Microtremor Measurements in the Nile Delta Basin, Egypt: Response of the Topmost Sedimentary Layer" by E. A. Fergany and S. Bonnefoy-Claudet. Seismological Research Letters ; 81 (2): 241–243. doi: https://doi.org/10.1785/gssrl.81.2.241.

NIBS. (2003). "Hazus MH MR4 Technical Manual." National Institute of Building Sciences, Department of Homeland Security, Emergency Preparedness and Response Directorate, Washington, D.C.

Noble, E. E., & Sanchez, P. P. (1993). A note on the information content of a consistent pairwise comparison judgment matrix of an AHP decision maker. *Theory and Decision*. *34*(2), 99-108.

Novelli, V., D'Ayala, D., Makhloufi, N., Benouar, D., & Zekagh, A. (2015). A procedure for the identification of the seismic vulnerability at territorial scale. Application to the Casbah of Algiers. *Bulletin of Earthquake Engineering, 13*(1), 177-202.

NRC/IRC. (1992). "Manual for screening of buildings for seismic investigation." National Research Council of Canada, Institute for Research in Construction, Ottawa, ON.

NRC/IRC. (2015). "National Building Code of Canada 2015." National Research Council of Canada, Institute for Research in Construction, Ottawa, ON.

Oaks, D. (1990). The damage assessment process: the application of ATC-20. *The Loma Prieta earthquake, studies of short-term impacts,* Institute of Behavioral Science, University of Colorado, Boulder, CO, 6-16.

Peiris, N., Rossetto, T., Burton, P., & Mahmoud, S. (2008). Kashmir Pakistand Earthquake of October 8 2005. A Field Report by EEFIT. In: Earthquake Engineering Field Investigation Team, Institution of Structural ….

Revkin, A. C. (2008). Earthquake in China highlights the vulnerability of schools in many countries. *New York Times.* doi:https://nyti.ms/2oPU14W

Rodgers, J. (2012). *Why schools are vulnerable to earthquakes.* Proceedings, 15th World Conference on Earthquake Engineering, Lisbon, pp. 24-28.

Rossetto, T., Gehl, P., Minas, S., Galasso, C., Duffour, P., Douglas, J., & Cook, O. (2016). FRACAS: A capacity spectrum approach for seismic fragility assessment including record-to-record variability. *Engineering Structures, 125*, 337-348.

Saaty, T. L. (1977). A scaling method for priorities in hierarchical structures. *Journal of mathematical psychology, 15*(3), 234-281.

Saaty, T. L. (2000). *Fundamentals of decision making and priority theory with the analytic hierarchy process* (Vol. 6): RWS publications.

Saaty, T. L. (2006). Rank from comparisons and from ratings in the analytic hierarchy/network processes. *European Journal of Operational Research, 168*(2), 557-570.

Sensquake. (2017). Sensequake, 3D-SAM. (2017). Software for ambient vibration test and seismic assessment of structural and non-structural components; 2017 <http://www.sensequake.com/>.

Singh, S., Reinoso, E., Arroyo, D., Ordaz, M., Cruz-Atienza, V., Pérez-Campos, X., . . . Hjörleifsdóttir, V. (2018). Deadly intraslab Mexico earthquake of 19 September 2017 (M w 7.1): Ground motion and damage pattern in Mexico City. *Seismological Research Letters, 89*(6), 2193-2203.

Taghavi, S., & Miranda, E. (2003). Response Assessment of Nonstructural Building Elements. PEER 2003/05, Pacific Earthquake Engineering Research Center. *University of California, Berkeley College of Engineering*.

Taskin, B., Sezen, A., Tugsal, U., & Erken, A. (2013). The aftermath of 2011 Van earthquakes: evaluation of strong motion, geotechnical and structural issues. *Bulletin of Earthquake Engineering, 11*(1), 285-312.

Tinawi, R., & Mitchell, D. (1990). *1988 Saguenay earthquake. Damage to schools and post-disaster buildings.* Engineering in our Environment: CSCE Annual Conference and 1st Biennial Environmental Speciality Conference.

Tischer, H. (2012). *Rapid seismic vulnerability assessment of school buildings in Québec. PhD. Department of Civil Engineering and Applied Mechanics* . McGill University , Montreal, QC. 258 p.

Tischer, H., Mitchell, D., & McClure, G. (2012). Comparison of North American Seismic Screening Methods Applied to School Buildings. *Journal of Civil Engineering and Architecture, 6*(7), 799.

Tummala, V. R., & Ling, H. (1998). A note on the computation of the mean random consistency index of the analytic hierarchy process (AHP). *Theory and decision, 44*(3), 221-230.

Tummala, V. R., & Wan, Y.-w. (1994). On the mean random inconsistency index of analytic hierarchy process (AHP). *Computers & Industrial Engineering*. *27*(1-4), 401-404.

Uppuluri, V. (1978). Logarithmic least-squares approach to Saaty's decision problems. *Mathematics and Statistics Research Department Progress Report*, 19-21.

Vamvatsikos, D., & Cornell, C. A. (2005). Direct estimation of seismic demand and capacity of multidegree-of-freedom systems through incremental dynamic analysis of single degree of freedom approximation. *Journal of Structural Engineering, 131*(4), 589-599.

Vicente, R., Parodi, S., Lagomarsino, S., Varum, H., & Silva, J. M. (2011). Seismic vulnerability and risk assessment: case study of the historic city centre of Coimbra, Portugal. *Bulletin of Earthquake Engineering, 9*(4), 1067-1096.